NEUROPHYSIOLOGY

An estrogen-sensitive hypothalamus-midbrain neural circuit controls thermogenesis and physical activity

Hui Ye[1], Bing Feng[2], Chunmei Wang[3], Kenji Saito[3]†, Yongjie Yang[3], Lucas Ibrahimi[1], Sarah Schaul[1], Nirali Patel[1], Leslie Saenz[1], Pei Luo[1], Penghua Lai[1], Valeria Torres[1], Maya Kota[1], Devin Dixit[1], Xing Cai[3], Na Qu[3], Ilirjana Hyseni[3], Kaifan Yu[3], Yuwei Jiang[4], Qingchun Tong[5], Zheng Sun[6], Benjamin R. Arenkiel[7], Yanlin He[2]*, Pingwen Xu[1,4]*, Yong Xu[3,8]*‡

Estrogen receptor–α (ERα) expressed by neurons in the ventrolateral subdivision of the ventromedial hypothalamic nucleus (ERα^vlVMH) regulates body weight in females, but the downstream neural circuits mediating this biology remain largely unknown. Here we identified a neural circuit mediating the metabolic effects of ERα^vlVMH neurons. We found that selective activation of ERα^vlVMH neurons stimulated brown adipose tissue (BAT) thermogenesis, physical activity, and core temperature and that ERα^vlVMH neurons provide monosynaptic glutamatergic inputs to 5-hydroxytryptamine (5-HT) neurons in the dorsal raphe nucleus (DRN). Notably, the ERα^vlVMH → DRN circuit responds to changes in ambient temperature and nutritional states. We further showed that 5-HT^DRN neurons mediate the stimulatory effects of ERα^vlVMH neurons on BAT thermogenesis and physical activity and that ERα expressed by DRN-projecting ERα^vlVMH neurons is required for the maintenance of energy balance. Together, these findings support a model that ERα^vlVMH neurons activate BAT thermogenesis and physical activity through stimulating 5-HT^DRN neurons.

INTRODUCTION

Estrogen, an ovarian hormone, has been shown to play a crucial role in body weight control in both animals and humans (1). Estrogen produces essential anti-obesity functions through decreasing food intake (2), increasing physical activity and energy expenditure (3), and modulating fat distribution (4). Estrogen's anti-obesity effects have been suggested to be primarily mediated by estrogen receptor–α (ERα), because genetic deletion of ERα in mice leads to obesity (4).

ERα in the brain plays a vital role in maintaining energy balance and body weight control. Two ERα-expressing neuronal populations essential for estrogenic regulation of body weight were identified in the hypothalamus. ERα expressed by pro-opiomelanocortin neurons in the arcuate hypothalamic nucleus (ARC) regulates food intake (5–7), while ERα in the ventrolateral subdivision of the ventral lateral ventromedial hypothalamic nucleus (vlVMH) modulates two components of energy expenditure, spontaneous physical activity and thermogenesis, in females (5, 8). The stimulatory effects of ERα^vlVMH on energy expenditure have been consistently observed in other studies. For example, stereotaxic delivery of 17β-estradiol (E2) into the vlVMH stimulates brown adipose tissue (BAT) thermogenesis in females (9). Ablation of ERα^vlVMH neurons induced by

NK2 homeobox transcription factor 1 (*NKX2-1*) knockout decreases physical activity and increases body weight in females (10). Together, these findings suggest that ERα^vlVMH neurons play a crucial role in estrogenic regulation of energy expenditure.

In addition to regulating energy expenditure, ERα^vlVMH neurons also modulate glucose homeostasis in females (11), as well as social investigation, mating, and aggression in both sexes (12–16). Distinct subpopulations of ERα^vlVMH neurons with nonoverlapping gene expression signatures have been recently identified (17, 18), partially explaining these diverse and sex-specific functions. However, the specific downstream neural circuits that mediate the metabolic functions of ERα^vlVMH neurons remain unknown.

Here, we aimed to identify the essential downstream neural populations mediating the metabolic effects of ERα^vlVMH neurons. Using cell type–specific anterograde and retrograde neuronal tracing methods, we identified 5-hydroxytryptamine (5-HT) neurons in the dorsal raphe nucleus (DRN, 5-HT^DRN) as one downstream neural population directly innervated by ERα^vlVMH neurons. Through channelrhodopsin-2 (ChR2) circuit mapping (CRACM) experiments, we confirmed the synaptic neurotransmission of these two neural nodes and further identified glutamate as the essential neurotransmitter at the ERα^vlVMH → 5-HT^DRN synapse. We further examined the functions of this glutamatergic ERα^vlVMH → 5-HT^DRN circuit in the regulation of thermogenesis and physical activity. Notably, we found that the ERα^vlVMH → DRN circuit also responded dynamically to changes in ambient temperature and nutritional state. Last, we demonstrated that ERα expressed by DRN-projecting ERα^vlVMH neurons is required for the physiological regulations of energy homeostasis in female mice.

RESULTS

Activation of ERα^vlVMH neurons stimulates BAT thermogenesis and physical activity

To begin to evaluate the effects of E2 on this circuit, we first tested the electrophysiological responses of identified ERα^vlVMH neurons

[1]Division of Endocrinology, Diabetes, and Metabolism, Department of Medicine, The University of Illinois at Chicago, Chicago, IL 60612, USA. [2]Pennington Biomedical Research Center, Louisiana State University System, Baton Rouge, LA 70808, USA. [3]Children's Nutrition Research Center, Department of Pediatrics, Baylor College of Medicine, Houston, TX 77030, USA. [4]Department of Physiology and Biophysics, The University of Illinois at Chicago, Chicago, IL 60612, USA. [5]Brown Foundation Institute of Molecular Medicine, University of Texas Health Science Center at Houston, Houston, TX 77030, USA. [6]Department of Internal Medicine, Baylor College of Medicine, Houston, TX 77030, USA. [7]Department of Molecular and Human Genetics, Baylor College of Medicine, Houston, TX 77030, USA. [8]Department of Molecular and Cellular Biology, Baylor College of Medicine, Houston, TX 77030, USA.
*Corresponding author. Email: yongx@bcm.edu (Y.X.); pingwenx@uic.edu (P.X.); yanlin.he@pbrc.edu (Y.H.)
†Present address: Department of Neuroscience and Pharmacology, Roy J. and Lucille A. Carver College of Medicine, The University of Iowa, Iowa City, IA, USA.
‡Lead author.

to E2 in ex vivo brain slices from ERα-ZsGreen mice. In this mouse model, ZsGreen is driven by the mouse ERα promoter and selectively expressed in ERα neurons (*19*). We started by measuring the effects of E2 on resting membrane potential and firing frequency of these green fluorescent neurons identified in the vlVMH (fig. S1, A and B). We found that E2 treatment significantly increased both resting membrane potential and firing frequency of ERα[vlVMH] neurons (Fig. 1, A to E). To block presynaptic inputs from afferent neurons, we preincubated brain slices with tetrodotoxin (TTX, a potent sodium channel blocker), 6-cyano-7-nitroquinoxaline-2,3-dione (CNQX, a competitive glutamate AMPA receptor antagonist), 2-amino-5-phosphopentanoic acid [D-AP5, a glutamate *N*-methyl-D-aspartate (NMDA) antagonist], and bicuculline [a competitive γ-aminobutyric acid type A (GABA_A) receptor antagonist]. In the presence of these blockers, E2 (100 nM) treatment still depolarized all recorded ERα[vlVMH] neurons (fig. S1, C to E), suggesting a direct stimulatory effect of E2 on ERα[vlVMH] neurons.

On the basis of these initial observations, we next used the designer receptors exclusively activated by designer drugs (DREADD) method to selectively activate ERα[vlVMH] neurons by stereotaxic injection of adeno-associated virus 2 (AAV2)-DIO-hM3Dq-mCherry into the vlVMH of Esr1-Cre mice (Fig. 1F). To exclude possible off-target effects of clozapine *N*-oxide (CNO) or its metabolites (*20*), we included wild-type (WT) + hM3Dq/saline, WT + hM3Dq/CNO, and Esr1-Cre + hM3Dq/saline mice as controls. We observed distinct expression of hM3Dq-mCherry in Esr1-Cre + hM3Dq but not in WT + hM3Dq mice (fig. S2A). As expected, CNO treatment increased both resting

membrane potential and firing frequency of hM3Dq-expressed ERα[vlVMH] neurons (fig. S2, B to D). We found that in females, acute stimulation of ERα[vlVMH] neurons induced by intraperitoneal injection of CNO significantly increased physical activity, as well as BAT and core temperature, suggesting an increased thermogenesis (Fig. 1, G to J). CNO-induced increases in physical activity lasted for 3 hours, while elevated BAT temperature persisted up to 6 hours following injection (Fig. 1, I and J). Notably, there was no difference in BAT thermogenesis and physical activity between WT + hM3Dq and Esr1-Cre + hM3Dq mice after saline injections (fig. S2, E and F). In addition, repeated activation of ERα[vlVMH] neurons in ovariectomized (OVX) female mice via daily CNO injections ameliorated high-fat diet (HFD)–induced body weight gain without affecting energy intake (Fig. 1, K and L), suggesting beneficial metabolic effects of ERα[vlVMH] activation.

We also noted similar observations in male WT + hM3Dq and Esr1-Cre + hM3Dq mice. We found that CNO-induced activation of ERα[vlVMH] neurons significantly increased both BAT thermogenesis and physical activity, while saline injections did not induce any effects (fig. S2, G to J). These findings indicate that ERα[vlVMH] neurons have similar metabolic regulatory effects in both females and males.

ERα[vlVMH] neurons monosynaptically innervate 5-HT[DRN] neurons

We previously reported that ERα[vlVMH] neurons send condensed projections to the DRN, which surround 5-HT[DRN] neurons (*11*). These findings suggest that ERα[vlVMH] neurons may synapse on
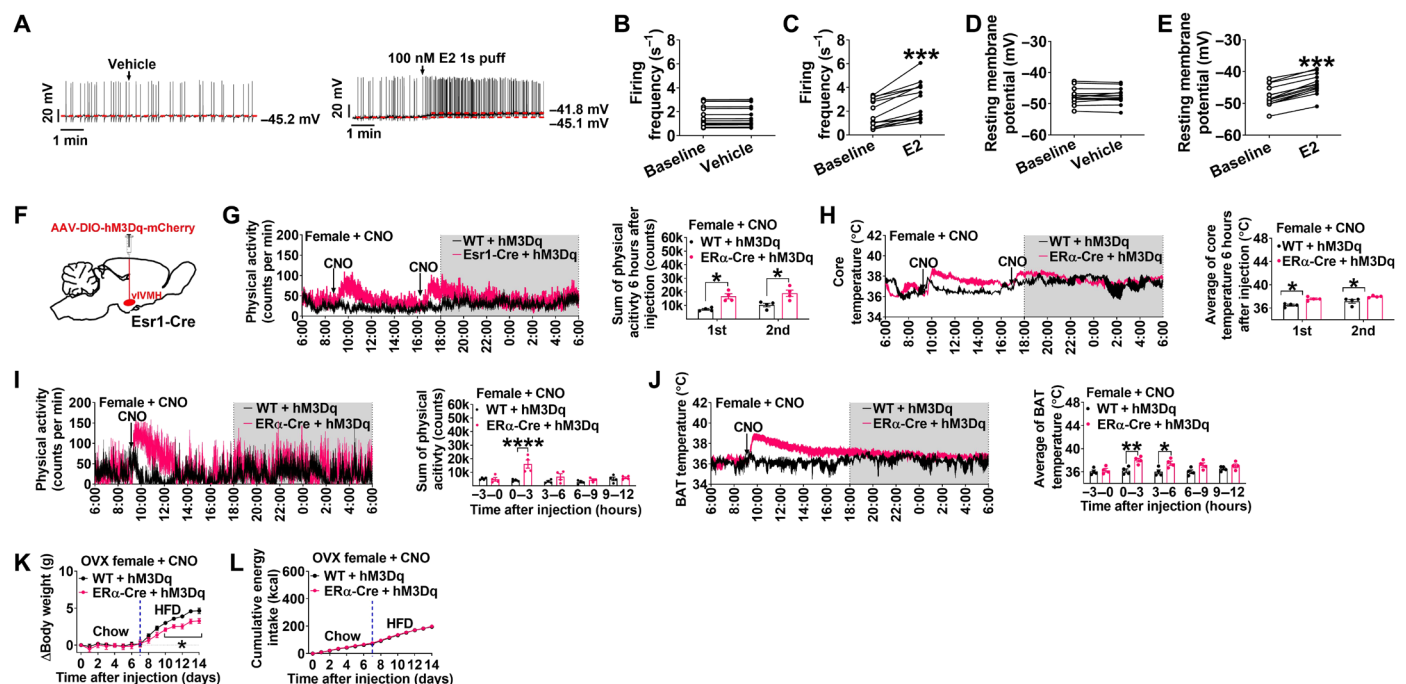

Fig. 1. Chemogenetic activation of ERα[vlVMH] neurons stimulates physical activity and BAT thermogenesis in females. (See also figs. S1 and S2.) (**A**) Representative trace of ERα-ZsGreen (+) neurons in the vlVMH of female mice treated with vehicle (1% dimethyl sulfoxide in saline) or 17β-estradiol (E2, 100 nM, 1s puff). (**B** to **E**) Summary of firing frequency (B and C) and resting membrane potential (D and E) (*n* = 13 or 14). (**F**) Schematic of the experimental strategy. (**G** and **H**) Effects of CNO (3 mg/kg) intraperitoneal injection on physical activity (G) and core temperature (H) in female mice with emitter intra-abdominally implanted (*n* = 4). (**I** and **J**) Effects of CNO injection on physical activity (I) and BAT temperature (J) in female mice with emitter implanted under BAT (*n* = 4). (**K** and **L**) Effects of chronic CNO treatment (twice/day, 3 mg/kg i.p. injection) on body weight gain (K) and energy intake (L) of ovariectomized (OVX) female mice (*n* = 3 or 4). (B to E) Data are presented for each cell. ***$P < 0.001$ in paired *t* tests. (G to L) Results are shown as means ± SEM. (G and H) *$P < 0.05$ in unpaired *t* tests. (I to L) *$P < 0.05$, **$P < 0.01$, and ****$P < 0.0001$ in two-way analysis of variance (ANOVA) analysis followed by post hoc Sidak tests.

5-HT^{DRN} neurons, which play an essential role in BAT thermogenesis (*21*). To establish the synaptic innervation between ERα^{vlVMH} neurons and 5-HT^{DRN} neurons, we stereotaxically injected anterograde trans-synaptic tracing virus Ad-iN/WED cre-inducible WGA adenoviral vector into the vlVMH of Esr1-Cre mice (Fig. 2A). Ad-iN/WED is a Cre-dependent virus that harbors a green fluorescent protein (GFP)–tagged wheat germ agglutinin (WGA) (*22*) and, following injection, was exclusively expressed in ERα^{vlVMH} neurons (Fig. 2B), and anterogradely translocated to downstream neural populations. Through this anterograde labeling approach, we found abundant WGA-GFP expression in the DRN. Notably, majority of the WGA-GFP (+) neurons in the DRN expressed 5-HT (Fig. 2, C to E). These observations strongly indicate that 5-HT^{DRN} neurons receive synaptic innervation from ERα^{vlVMH} neurons.

WGA has also been reported to exhibit both retrograde transsynaptic transport (*23*), and multisynaptic transport of WGA has also been observed (*24*). Therefore, WGA tracing alone could not fully establish a direct projection from ERα^{vlVMH} neurons to 5-HT^{DRN} neurons. To confirm that ERα^{vlVMH} neurons provide monosynaptic inputs to DRN neural populations, we also used a rabies-mediated retrograde tracing system, including an EnvA-pseudotyped glycoprotein (G)–deleted Rabies-mCherry and Cre-dependent helper AAV virus AAV2-EF1a-FLEX-GT [enhanced GFP (EGFP) +

TVA]. EnvA-pseudotyped rabies virus does not infect neurons in the absence of the avian TVA (the cellular receptor for subgroup A avian leukosis viruses) receptor protein (*25*). Toward this, we first delivered AAV2-EF1a-FLEX-GT (EGFP + TVA) into the vlVMH of Esr1-Cre mice to induce TVA expression exclusively in ERα^{vlVMH} neuron cell bodies and fiber terminals. Subsequently, we introduced EnvA-G–deleted Rabies-mCherry into the downstream DRN brain region, where the fiber terminals of ERα^{vlVMH} neurons are located. The selective expression of TVA in ERα^{vlVMH} neurons allows for rabies infection of ERα^{vlVMH} neuronal fiber terminals and subsequent labeling of the cell bodies within the vlVMH (Fig. 2, F to I). We found that Rabies-mCherry expressed and colocalized with TVA-GFP in the vlVMH of the Esr1-Cre mouse (Fig. 2, J to L), confirming monosynaptic inputs from ERα^{vlVMH} neurons to the DRN neural populations.

A similar rabies-mediated retrograde tracing was performed to confirm further that vlVMH neurons provide monosynaptic inputs to Tryptophan Hydroxylase 2 (TPH2)^{DRN} neurons (fig. S3A). Specifically, we delivered AAV2-EF1a-FLEX-GTB (EGFP + TVA + rabies B19 glycoprotein) into the DRN of TPH2-iCreER/Rosa26-LSL-tdTOMATO mice to induce TVA and glycoprotein expression exclusively in TPH2^{DRN} neurons (fig. S3, B to D). Subsequently, we introduced EnvA-G–deleted Rabies-mCherry into the same DRN brain region.
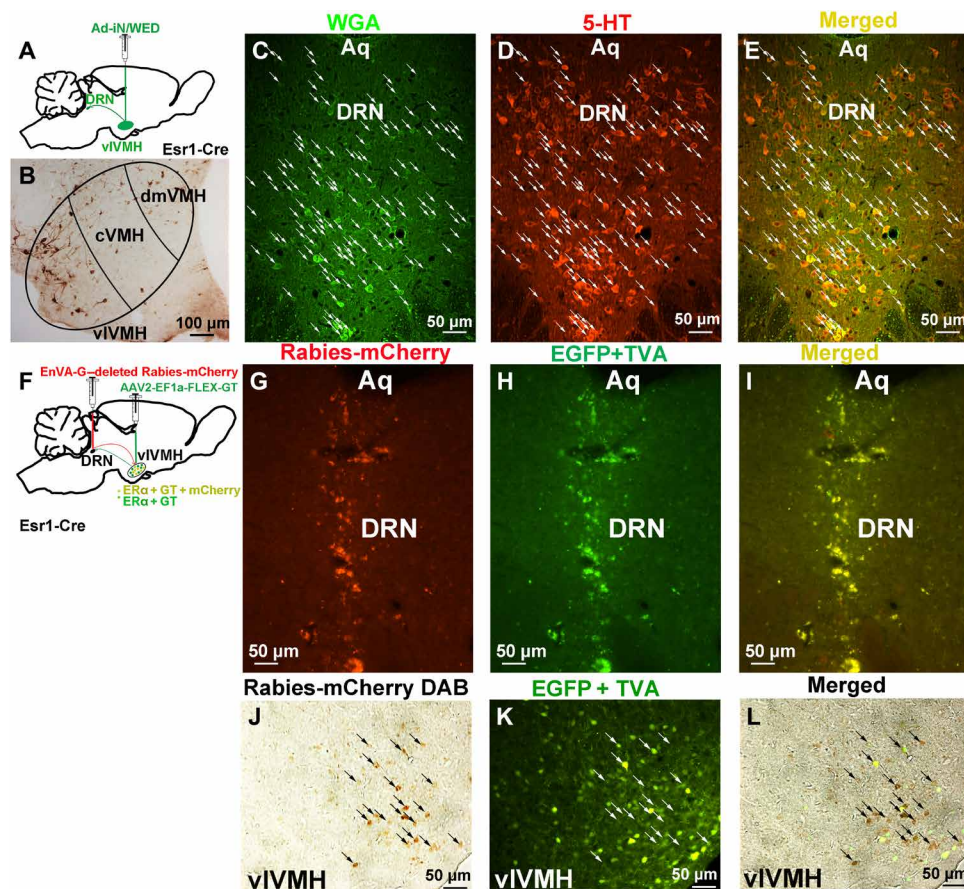

Fig. 2. ERα^{vlVMH} neurons provide monosynaptic innervation to 5-HT^{DRN} neurons. (See also fig. S3.) (**A**) Schematic of the experimental strategy using the Ad-iN/WED virus as a trans-synaptic anterograde tracer to identify the ERα^{vlVMH} → 5-HT^{DRN} circuit. (**B**) WGA immunoreactivity in the vlVMH of female Esr1-Cre mice. (**C** to **E**) Immunoreactivity of WGA (C, green), 5-HT (D, red), and merger (E, yellow) in the DRN. White arrows point to yellow dual fluorescent neurons. Aq, aqueduct. (**F**) Schematic of the experimental strategy using the EnvA-G–deleted Rabies-mCherry virus as a retrograde tracer to identify the ERα^{vlVMH} → DRN circuit. (**G** to **I**) Fluorescence of Rabies-mCherry (G, red), EGFP + TVA (H, green), and merger (I, yellow) in the DRN. (**J** to **L**) Immunoreactivity of Rabies-mCherry (J, brown), EGFP + TVA (K, green), and merger (L, yellow) in the vlVMH of female Esr1-Cre mice.

Glycoprotein is required for the retrograde trans-synaptic tracing of the rabies virus. The selective expression of TVA and glycoprotein in TPH2^{DRN} neurons allows for rabies infection of TPH2^{DRN} neurons and subsequent labeling of the upstream neurons providing monosynaptic inputs to TPH2^{DRN} neurons. We found that Rabies-mCherry expressed in multiple brain regions, including the ARC, the medial amygdala, the suprachiasmatic nucleus, the medial posterior part of the Arc, and vlVMH (fig. S3, E to L), confirming monosynaptic inputs from vlVMH neurons to the TPH2^{DRN} neural populations.

ERα^{vlVMH} neurons stimulate 5-HT^{DRN} neurons through glutamatergic neurotransmission

We next sought to target both ERα^{vlVMH} neurons and 5-HT^{DRN} neurons in the same mice. For the latter population, we used a knock-in TPH2-iCreER mouse allele. TPH2 is an essential enzyme for the synthesis of 5-HT in the brain, and we previously confirmed that TPH2-iCreER drives selective Cre activity in 5-HT neurons within the DRN (26). Using the TPH2-iCreER deliver line, upon tamoxifen induction produced robust Cre activity in the DRN (fig. S4A); no Cre activity was observed in the vlVMH (fig. S4B). Notably, Esr1-Cre mice show Cre activity in the DRN as reported by Cre-driven mCherry expression; however, the mCherry-positive neurons in the DRN were identified to be TPH neurons (fig. S4, C to E). Consistent with our previous findings, we confirmed that all ERα-expressing cells within the DRN are 5-HT neurons (26). In other words, the Esr1-Cre did not induce Cre activity in non–5-HT neurons in the DRN. Thus, within the DRN of the compound TPH2-iCreER/Esr1-Cre mice, Cre activity was exclusively induced in 5-HT neurons.

We next generated Esr1-Cre/TPH2-iCreER/Rosa26-LSL-tdTOMATO mice and stereotaxically injected both AAV2-DIO-ChR2-EYFP (enhanced yellow fluorescent protein) and Ad-iN/WED into the vlVMH (Fig. 3A). In these mice, the blue light–sensitive photoreceptor ChR2 was expressed in ERα^{vlVMH} neurons and their fiber terminals. WGA-GFP labeled ERα^{vlVMH} neurons and their downstream neurons (including those in the DRN), and therefore, tdTOMATO(+)WGA-GFP(+) neurons in the DRN were identified as the putative ERα^{vlVMH}-innervated 5-HT^{DRN} neurons (fig. S4, F to H). Consistent with the colocalization analysis of WGA-GFP and 5-HT in the DRN, most of the WGA-GFP(+) neurons were also tdTOMATO (+) (Fig. 3, B and C). To characterize the synaptic transmission within the ERα^{vlVMH} → 5-HT^{DRN} neural circuit, we used CRACM (27) to record light-induced responses of tdTOMATO(+)WGA-GFP(+) neurons in the DRN following blue light photostimulation of ChR2-expressing ERα^{vlVMH} fibers/terminals within the DRN (fig. S4, I to K).

Under the current clamp, we found that photostimulation significantly increased the resting membrane potential of tdTOMATO(+) WGA-GFP(+) neurons in the presence of TTX (Fig. 3, D and E). Together, these data suggest a direct excitatory input from ERα^{vlVMH} neurons to 5-HT^{DRN} neurons. Under voltage-clamp conditions, we detected light-evoked excitatory postsynaptic currents (eEPSCs) in most tdTOMATO(+)WGA-GFP(+) neurons tested (70.59% eEPSC versus 29.41% no eEPSC in total 17 neurons; Fig. 3, F and G). Notably, no eEPSCs were detected in tdTOMATO(+)WGA-GFP(−) neurons (Fig. 3H), validating the high fidelity of this WGA-GFP–assisted CRACM approach. After blocking presynaptic inputs by 4-aminopyridine (4-AP) and TTX preincubation, the amplitude and latency of eEPSCs remained unchanged (Fig. 3, I and J). These findings revealed a monosynaptic response induced by blue light, which was consistent with the current-clamp results. We also found that blue light–induced eEPSCs were blocked by incubation of D-AP5 (an NMDA receptor antagonist) + CNQX (an AMPA receptor antagonist), confirming their glutamatergic nature (Fig. 3, F and I). In summary, our results suggest that the ERα^{vlVMH} neurons provide monosynaptic glutamatergic inputs to 5-HT^{DRN} neurons.
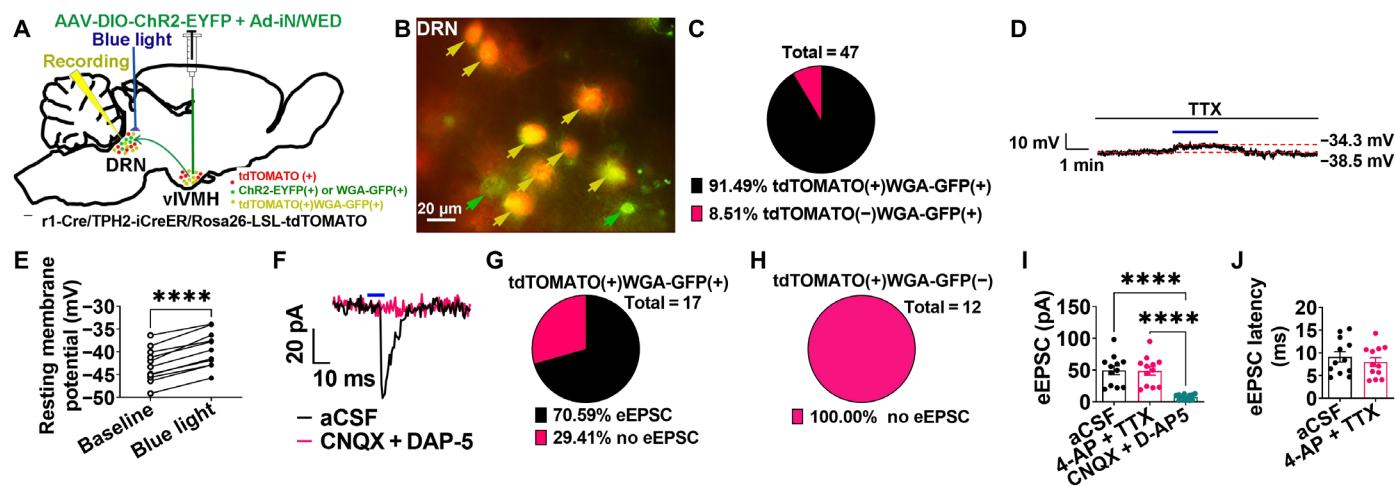
Fig. 3. ERα^{vlVMH} → DRN neural circuit stimulates 5-HT^{DRN} neurons through glutamatergic neurotransmission. (See also figs. S4 and S5.) (**A**) Schematic of the experimental strategy. (**B** and **C**) A representative image (B) and a summary (C) of yellow arrow–pointed tdTOMATO(+)WGA-GFP(+) and green arrow–pointed tdTOMATO(−)WGA-GFP(+) neurons in the DRN. (**D** and **E**) Representative trace (D) and summary (E) of tdTOMATO(+)WGA-GFP(+) neurons in the DRN responding to blue light photostimulation in the DRN (20 Hz, 10 ms per pulse, and 3 mW for 2 min) in the presence of 1 μM TTX (n = 11). (**F**) Representative eEPSC induced by blue light photostimulation (10 ms, 3-mW stimulation) after preincubation of artificial cerebrospinal fluid (aCSF) or 30 μM CNQX + 30 μM AP-5 in tdTOMATO(+)WGA-GFP(+) neurons in the DRN. (**G** and **H**) Summary of eEPSC in tdTOMATO(+)WGA-GFP(+) (G) and tdTOMATO(+)WGA-GFP(−) neurons (H). (**I**) Summary of eEPSC amplitude in the presence of aCSF, 1 μM 4-aminopyridine (4-AP) + 1 μM TTX, or CNQX + D- AP5 (n = 12). (**J**) Summary of eEPSC latency in the presence of aCSF or 4-AP + TTX (n = 12). (E) Data are presented for each cell. ****$P < 0.0001$ in paired t tests. (I and J) Results are presented as means ± SEM. ****$P < 0.0001$ in repeated-measures ANOVA analysis followed by post hoc Dunnett's tests.

To further characterize the synaptic transmission between ERα^{vlVMH} and 5-HT(−)^{DRN} downstream neural populations, the same current clamp was also performed in tdTOMATO(−)WGA-GFP(+) neurons. We detected eEPSCs in most tdTOMATO(−)WGA-GFP(+) neurons tested (72.00% eEPSC versus 28.00% no eEPSC in total 25 neurons; fig. S5, A and B). Notably, the amplitude and latency of eEPSCs remained unchanged after 4-AP and TTX preincubation (fig. S5, C and D). However, eEPSCs were blocked by incubation of D-AP5 + CNQX, suggesting glutamatergic transmission (fig. S5, A and C). Collectively, our data support that the ERα^{vlVMH} neurons provide monosynaptic glutamatergic inputs to both 5-HT(+) and 5-HT(−) DRN neurons.

ERα^{vlVMH} → DRN neural circuit responds to changes in ambient temperature and nutritional state

To test the physiological relevance of the ERα^{vlVMH} → DRN neural circuit, we next recorded the neural dynamics of identified DRN-projecting ERα^{vlVMH} neurons during temperature or nutritional changes. Toward this, we injected a retrogradely transported CAV2-Cre virus into the DRN of ERα-ZsGreen/Rosa26-LSL-tdTOMATO mice (Fig. 4A). In this case, CAV2-Cre retrogradely infected

upstream ERα^{vlVMH} neurons that project to the DRN and induced tdTOMATO (red) expression. Thus, DRN-projecting ERα^{vlVMH} neurons were labeled with tdTOMATO(+)ZsGreen(+)dual fluorescent colors (fig. S6, A to C). We next performed current-clamp recordings in identified yellow neurons in brain slices that were prepared from mice exposed to different ambient temperatures. We found that the firing frequency of the DRN-projecting ERα^{vlVMH} neurons was increased in mice exposed to cold (4°C) and decreased with warm exposure (40°C; Fig. 4, B and C). Resting membrane potential was not significantly altered by the cold exposure but was significantly decreased by warm exposure (Fig. 4D). These results revealed thermosensing capabilities of DRN-projecting ERα^{vlVMH} neurons, where low ambient temperatures activate and high temperatures inhibit these neurons. We further investigated the thermosensing properties of DRN-projecting ERα^{vlVMH} neurons in OVX female mice with depleted endogenous ovarian hormones. Notably, OVX abolished the responses of firing frequency and resting membrane potential to changes in ambient temperature (Fig. 4, B to D), indicating that ovarian hormones (including estrogen) are required for thermosensing capabilities of DRN-projecting ERα^{vlVMH} neurons.
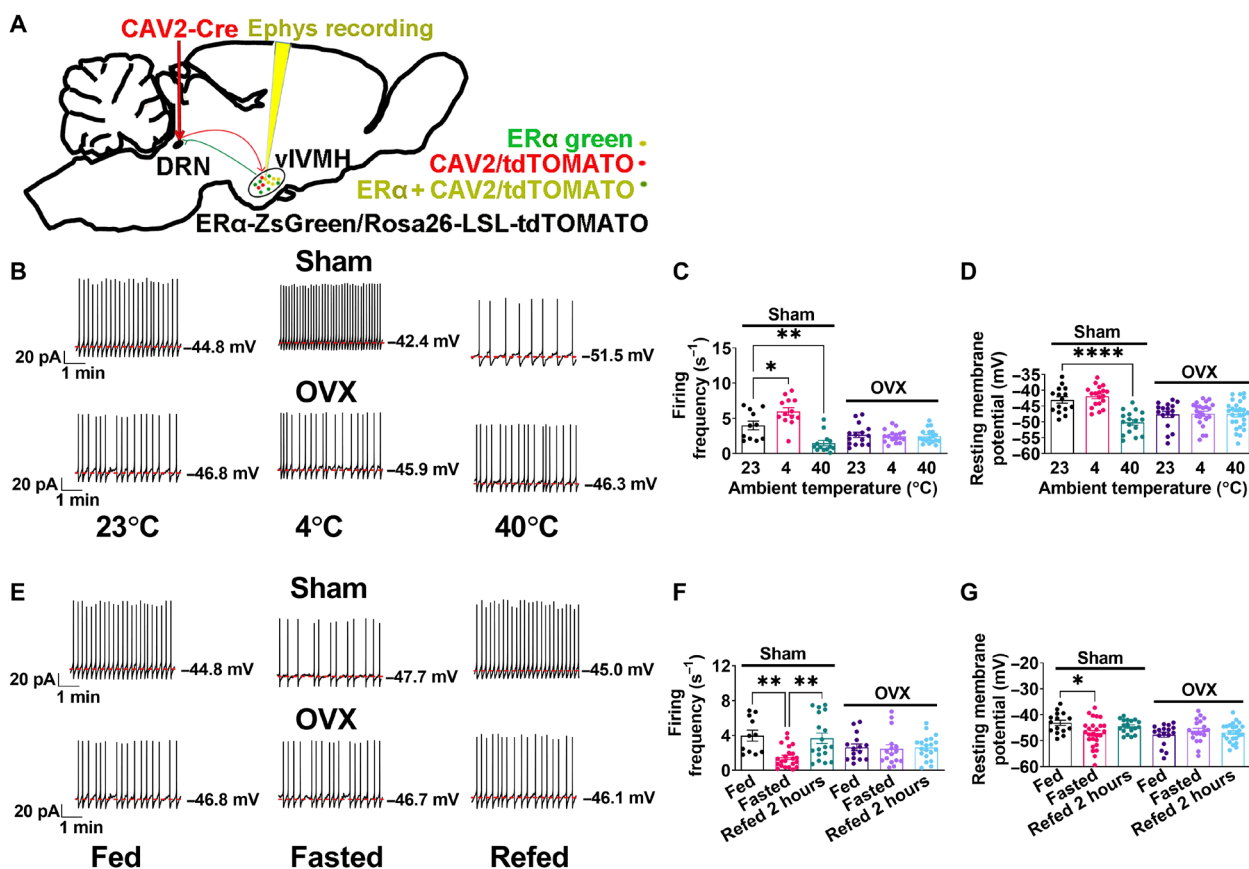

Fig. 4. Neural dynamics of DRN-projecting ERα^{vlVMH} neurons. (See also fig. S6.) (**A**) Schematic of the experimental strategy using the CAV2-Cre virus to label and record the electrophysiological response of DRN-projecting ERα^{vlVMH} neurons in Sham or OVX female ERα-ZsGreen/Rosa26-LSL-tdTOMATO mice. (**B**) Representative responses to the exposure to room temperature (23°C), 4°C, or 40°C for 30 min in DRN-projecting ERα^{vlVMH} neurons labeled with dual yellow fluorescent colors (ZsGreen + tdTOMATO) in Sham or OVX female mice. (**C** and **D**) Summary of firing frequency (C) and resting membrane potential (D) when exposed to different temperatures ($n = 11$, 13, 13, 15, 17, or 18). (**E**) Representative response to fed condition, 24-hour fasting, or 2-hour refeeding after 24-hour fasting in DRN-projecting ERα^{vlVMH} neurons in Sham or OVX female mice. (**F** and **G**) Summary data of firing frequency (F) and resting membrane potential (G) under different metabolic conditions ($n = 11$, 22, 18, 15, 16, or 20). (C, D, F, and G) Results are presented as means ± SEM. *$P < 0.05$, **$P < 0.01$, and ****$P < 0.0001$ in one-way ANOVA analysis followed by post hoc Dunnett's tests.

We then tested responses of DRN-projecting ERα[vlVMH] neurons to fasting and refeeding. We found that the firing frequency of DRN-projecting ERα[vlVMH] neurons was decreased by fasting and increased by refeeding, and the resting membrane potential of these neurons was decreased by fasting (Fig. 4, E to G). These neural responses associated with animals' feeding conditions were also blocked in OVX female mice (Fig. 4, E to G). We next further tested the responses of non-DRN–projecting ERα[vlVMH] tdTOMATO(−) ZsGreen(+) neurons. While DRN-projecting ERα[vlVMH] neurons were sensitive to changes in ambient temperature and nutritional state, these non-DRN–projecting ERα[vlVMH] neurons only showed responses to fasting challenge (fig. S6, D to G).

The stimulatory effects of ERα[vlVMH] → DRN circuit on BAT thermogenesis and physical activity are independent of ADRB3

To further test the metabolic effects of the ERα[vlVMH] → DRN circuit, we selectively activated this circuit using ChR2-mediated photostimulation. More specifically, we stereotaxically injected Cre-dependent AAV2-DIO-ChR2-EYFP into the vlVMH of Esr1-Cre mice and implanted an optic fiber above the DRN (Fig. 5A and fig. S7A). Blue light stimulation (473 nm, 10 ms per pulse, 20 Hz, 3-s on, and 2-s off for 1 hour) of the DRN resulted in significant increases in both BAT temperature and physical activity compared to the same mice receiving control yellow light pulses (473 nm, 10 ms per pulse, 20 Hz, 3-s on, and 2-s off for 1 hour) during the same time of the day (Fig. 5, B, D, E, and G). Notably, post hoc staining of EYFP

and cFOS (Fos proto-oncogene, AP-1 transcription factor subunit) and electrophysiology confirmed accurate injection/implantation and targeted activation of ERα[vlVMH] neurons (fig. S7, B to E). These findings indicate that activation of the ERα[vlVMH] → DRN circuit is sufficient to stimulate BAT thermogenesis and physical activity.

To explore the peripheral mechanisms underlying this action, we next intraperitoneally injected mice with SR59230A, a β3-adrenergic receptor (ADRB3) antagonist, before photostimulation. As previously reported (28), SR59230A showed inhibitory effects on the baseline BAT thermogenesis and physical activity (fig. S7, E and F). However, pretreatment of SR59230A did not affect photostimulation effects on BAT thermogenesis or physical activity (Fig. 5, C, D, F, and G). Together, these results indicate that the stimulatory effects of the ERα[vlVMH] → DRN neural circuit on BAT thermogenesis and physical activity are independent of ADRB3.

Inhibition of ERα[vlVMH] → DRN circuit reduces BAT thermogenesis and core temperature

To evaluate the in vivo physiological role of the ERα[vlVMH] → DRN circuit, we adopted a selective chloride-conducting channelrhodopsin (iC++) approach to inhibit this circuit. As before, we stereotaxically injected AAV-DIO-iC++-EYFP into the vlVMH of Esr1-Cre mice and implanted optic fibers to target the DRN, followed by blue light stimulation to inhibit the ERα[vlVMH] → DRN projection (Fig. 5H). Inhibition of the ERα[vlVMH] → DRN circuit by blue light pulses (473 nm, 10 ms per pulse, 20 Hz, 3-s on, and 2-s off for 1 hour) decreased BAT thermogenesis and core temperature without changing physical
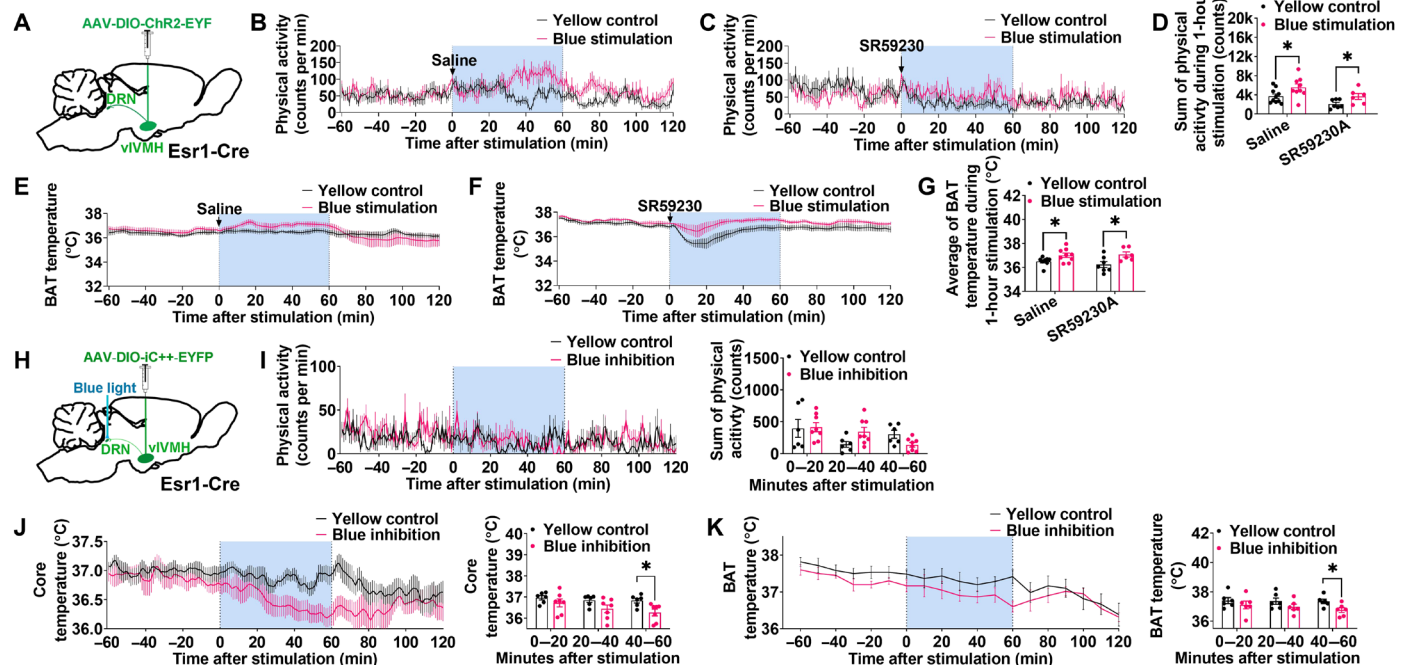

Fig. 5. ERα[vlVMH] → 5-HT[DRN] circuit stimulates both BAT thermogenesis and physical activity. (See also figs. S7 and S8.) (**A**) Schematic of the experimental strategy. (**B** to **D**) Effects of yellow or blue light stimulation (589 or 473 nm, 10 ms per pulse, 20 Hz, 3-s on, and 2-s off for 1 hour) in the DRN on physical activity. Female mice were intraperitoneally injected with saline (n = 10 or 10) or SR59230 (0.5 mg/kg, n = 7 or 7) in the beginning of light stimulation. (**E** to **G**) Effects of yellow or blue light stimulation in the DRN on BAT temperature (n = 10, 10, 7, or 7). (**H**) Schematic of the experimental strategy. (**I**) Effects of yellow or blue light stimulation (589 or 473 nm, 10 ms per pulse, 20 Hz, 3-s on, and 2-s off for 1 hour) in the DRN on physical activity (n = 8 or 8). (**J**) Effects of yellow or blue light stimulation in the DRN on core temperature (n = 6 or 7). (**K**) Effects of yellow or blue light stimulation in the DRN on BAT temperature (n = 6 or 7). All data are presented as means ± SEM. *P < 0.05 in unpaired t tests.

activity, compared to the same mice receiving yellow light pulses (473 nm, 10 ms per pulse, 20 Hz, 3-s on, and 2-s off for 1 hour) (Fig. 5, I to K). Notably, the observed inhibitory effects on both BAT and core temperature were observed following 40 min of blue light photostimulation, suggesting that the DRN is an essential downstream brain region for metabolic effects of ERα^{vlVMH} neurons. The accuracy of injections and implantations was always validated by IHC of EYFP following experimentation (fig. S8, A and B). We further demonstrated that both resting membrane potentials and firing frequency of iC++-positive ERα^{vlVMH} neurons were significantly reduced by blue light exposure at the vlVMH (473 nm, 10 ms per pulse, and 20 Hz for 3 min) (fig. S8, C to G). These results indicate that the baseline activity of the ERα^{vlVMH} → DRN circuit is required for the normal maintenance of BAT thermogenesis and core temperature.

Glutamatergic neurotransmission is required for the stimulatory effects of ERα^{vlVMH} → DRN circuit on BAT thermogenesis and physical activity

To directly examine the contribution of glutamate signaling on the metabolic effects of ERα^{vlVMH} → DRN circuit, we injected Esr1-Cre female mice with AAV2-DIO-hM3Dq-mCherry into the vlVMH and then locally injected CNO with or without the glutamate receptor antagonist D-AP5 and CNQX into the DRN (Fig. 6A). CNO delivery to the DRN stimulated both physical activity and BAT thermogenesis, while coinjecting D-AP5 and CNQX into the DRN completely abolished these effects (Fig. 6, B and C). Therefore, we confirmed that ERα^{vlVMH} neurons stimulate BAT thermogenesis and physical activity through the activation of DRN downstream neurons in a glutamate-dependent manner.

The stimulatory effects of ERα^{vlVMH} neurons on BAT thermogenesis and physical activity are mediated by activation of 5-HT^{DRN} neurons

To directly test whether 5-HT^{DRN} neurons mediate the metabolic functions of ERα^{vlVMH} neurons, we next used dual DREADD technology to stimulate ERα^{vlVMH} neurons while simultaneously inhibiting 5-HT^{DRN} neurons (Fig. 6D). Combining Esr1-Cre/TPH2-iCreER mice and Cre-dependent AAV vectors, DREADD hM3Dq was targeted for expression in ERα^{vlVMH} neurons, while inhibitory DREADD hM4Di was expressed in 5-HT^{DRN} neurons (fig. S9, A to E). After CNO treatment, both resting membrane potential and firing frequency were increased in the ERα^{vlVMH} neurons and decreased in 5-HT^{DRN} neurons (fig. S9, F to K), confirming CNO-induced activation of ERα^{vlVMH} neurons and inhibition of 5-HT^{DRN} neurons. Possible metabolic contributions of nonspecific effects of CNO were excluded, as demonstrated by unchanged BAT thermogenesis and physical activity in WT + hM3Dq mice after CNO intraperitoneal injections (Fig. 6, E, I, J, and N). In Esr1-Cre + hM3Dq mice, CNO injections induced robust increases in BAT thermogenesis and physical activity compared to saline injections in the same mice (Fig. 6, F, I, K, and N). The observed stimulatory effects were significantly attenuated by the inhibition of 5-HT^{DRN} neurons in dual DREADD mice (Fig. 6, H, I, M, and N). Together, these data support that activation of 5-HT^{DRN} neurons is required for increased BAT thermogenesis and physical activity induced by activation of ERα^{vlVMH} neurons. Notably, inhibition of 5-HT^{DRN} neurons alone inhibited BAT thermogenesis but not physical activity (Fig. 6, G, I, L, and N).

ERα expressed by DRN-projecting ERα^{vlVMH} neurons is required for regulation of BAT thermogenesis, physical activity, and body weight

To further test the physiological functions of ERα^{vlVMH} → DRN neural circuit, we delivered ΔG Rabies FLPo-dsRedXpress and AAV-hSyn1-frEX-Cre-GFP to the DRN and vlVMH, respectively, of female Esr1$^{flox/flox}$ mice to retrogradely delete ERα from ERα^{vlVMH} → DRN neurons. In this setting, retrograde Rabies FLPo-dsRed was taken up by fiber terminals in the DRN and retrogradely transported to the vlVMH cell bodies, and AAV-hSyn1-frEX-Cre-GFP virus selectively expresses Cre recombinase only in flpo-expressing cells (see fig. S10, A and B for validation of this vector). Thus, Cre was expressed exclusively in DRN-projecting vlVMH neurons, resulting in deletion of ERα selectively in this subset of neurons (Fig. 7A). Notably, the overall number of cells in the vlVMH did not change after deletion as indicated by 4′,6-diamidino-2-phenylindole staining (fig. S10C), excluding the possibility of rabies-induced cytotoxicity or apoptosis. The specificity of deletion was first validated by dsRed, EGFP, and ERα immunohistochemistry (fig. S10, D to G). We found that ERα$^{vlVMH-DRN-KO}$ mice showed significantly decreased ERα-expressing neurons in the vlVMH compared to control mice (Fig. 7, B to D). Only a subset of vlVMH neurons in ERα$^{vlVMH-DRN-KO}$ mice lost ERα expression, consistent with selective deletion of ERα only from the DRN-projecting ERα^{vlVMH} neurons. Consistent with the metabolic effects caused by ERα^{vlVMH} → DRN circuitry manipulations, retrograde deletion of ERα from DRN-projecting ERα^{vlVMH} neurons led to decreased BAT thermogenesis and physical activity in female mice (Fig. 7, E and F). Notably, the experimental mice also showed increased body weight gain after 2 weeks of HFD feeding without affecting energy intake (Fig. 7, G and H). These results demonstrate that ERα expressed by DRN-projecting ERα^{vlVMH} neurons is physiologically relevant for the regulation of both BAT thermogenesis and physical activity in female mice.

DISCUSSION

Estrogen/ERα signaling in the vlVMH is vital for energy homeostasis and body weight control. The stimulatory effects of ERα^{vlVMH} on BAT thermogenesis have been consistently vetted in several studies using transgenic mouse models. Conditional knockout of ERα in the vlVMH using SF1-Cre lowers BAT thermogenesis in female mice and yields abdominal obesity, suggesting that ERα^{vlVMH} neurons stimulate energy expenditure to decrease adiposity (5). This mechanism of estrogenic control of body weight is further supported by the evidence that vlVMH-specific injection of E2 stimulates BAT thermogenesis by inhibiting adenosine monophosphate–activated protein kinase in the vlVMH (9). Notably, ERα^{vlVMH} neurons have also been shown to stimulate physical activity. For example, short hairpin RNA–induced ERα knockdown in the vlVMH decreases not only diet-induced thermogenesis but also physical activity, which results in obesity (8). Consistently, conditional knockout of Nkx2-1 using SF1-Cre leads to loss of ERα^{vlVMH} neurons, decreased physical activity, and obesity (10), suggesting stimulatory effects of ERα^{vlVMH} neurons on physical activity. Thus, ERα^{vlVMH} neurons represent a unique subpopulation capable of controlling both BAT thermogenesis and physical activity, at least in female animals.

Supporting this notion, a recent study confirmed that acute activation of ERα^{vlVMH} neurons enhances energy expenditure by increasing BAT thermogenesis and physical activity (17). We replicated
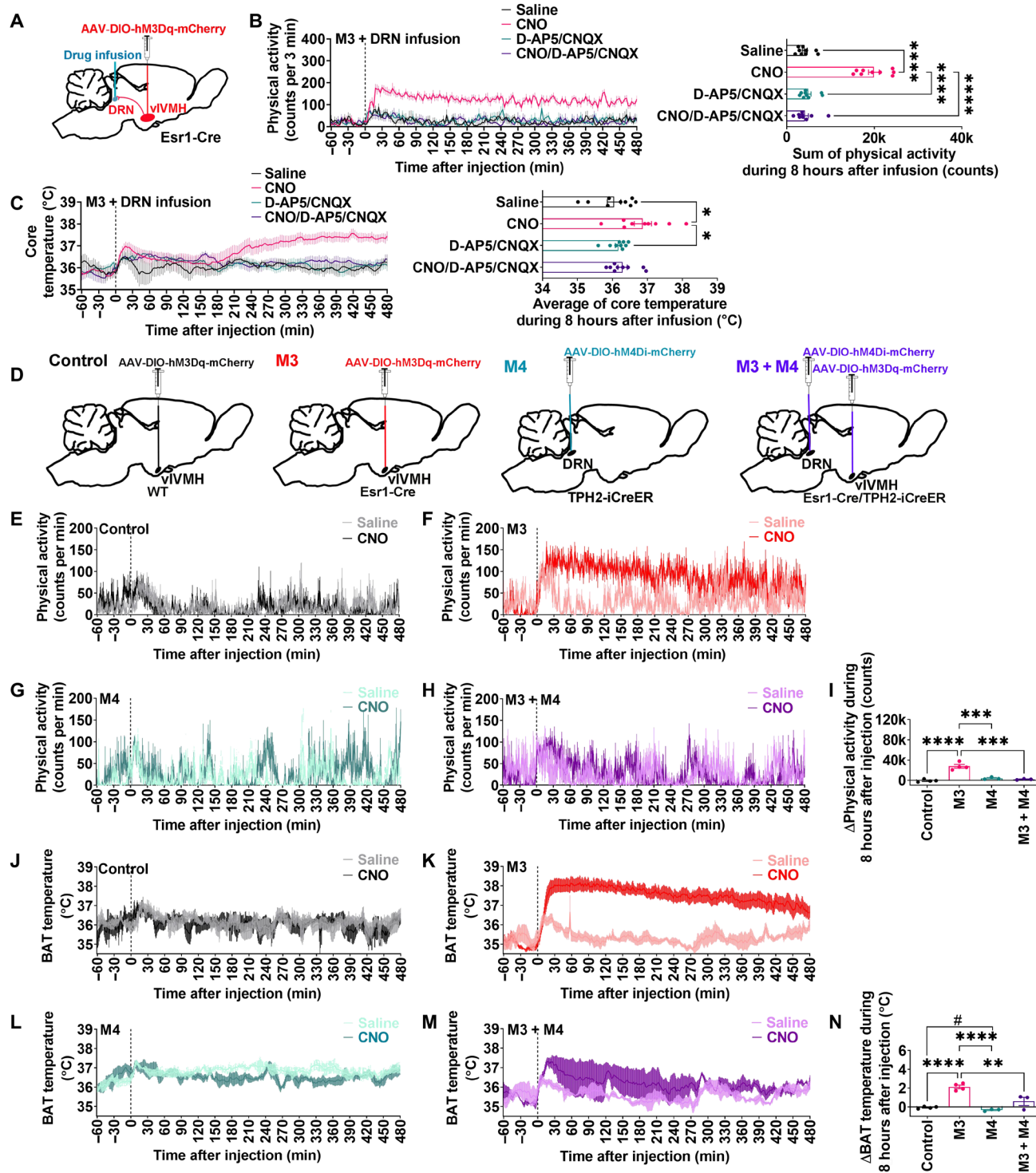
Fig. 6. The stimulatory effects of ERα^vlVMH neurons on BAT thermogenesis and physical activity are mediated by activation of 5-HT^DRN neurons through glutamatergic transmission. (See also fig. S9.) (**A**) Schematic of the experimental strategy. (**B** and **C**) Effects of 400 nl of DRN-specific infusion of saline, CNO (1 µg/µl), CNO (1 µg/µl) + D-AP5 (6.25 µg/µl) + CNQX (2.5 µg/µl), or D-AP5 (6.25 µg/µl) + CNQX (2.5 µg/µl) on physical activity (B) and core temperature (C) ($n = 9$). (**D**) Schematic of the experimental strategy. (**E** to **I**) Effects of saline or CNO (3 mg/kg) intraperitoneal injection on physical activity (E to H) and differences in the sum of physical activity between saline- and CNO-injected mice (I). (**J** to **N**) Effects of saline or CNO intraperitoneal injection on BAT temperature (J to M) and differences in the average of BAT temperature between saline- and CNO-injected mice (N) (control, $n = 4$; M3, $n = 4$; M4, $n = 3$; M3 + M4, $n = 3$). All data are presented as means ± SEM. *$P < 0.05$, **$P < 0.01$, ***$P < 0.001$, and ****$P < 0.0001$ in one-way ANOVA analysis followed by post hoc Tukey tests. #$P < 0.05$ in unpaired t tests.

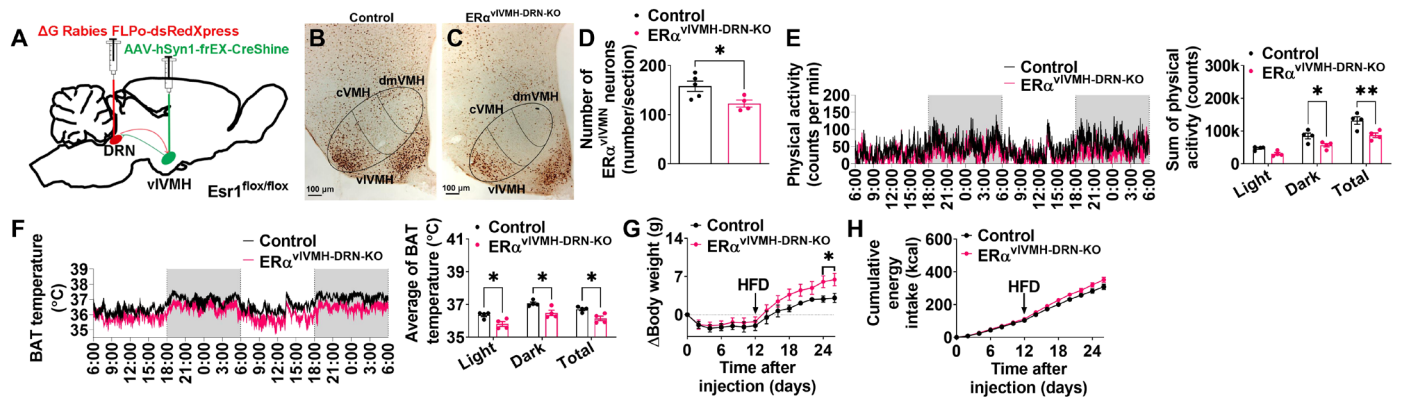**Fig. 7. ERα expressed by ERα^vlVMH → DRN neurons is required for estrogenic stimulation on BAT thermogenesis and physical activity.** (See also fig. S10.) (**A**) Schematic of the experimental strategy using the retrograde ΔG-Rabies-FLPo-dsRedXpress and FLPo-dependent AAV-hSyn1-frEX-Cre-GFP viruses to selectively delete ERα from DRN-projecting ERα^vlVMH neurons in the female Esr1^flox/flox mice (ERα^vlVMH-DRN-KO). Control group is female Esr1^flox/flox mice injected with AAV-CMV-GFP virus into the DRN and AAV-hSyn1-frEX-Cre-GFP virus into the vlVMH. (**B** and **C**) Immunohistochemistry staining of ERα in the vlVMH of female control (B) and ERα^vlVMH-DRN-KO (C) mice. (**D**) Average of ERα-expressing neurons in the vlVMH ($n = 5$ or 4). (**E**) Physical activity (left) and sum of physical activity during light, dark, or 48 hours recording (right) ($n = 4$). (**F**) BAT temperature (left) and average of BAT temperature during light, dark, or 48 hours of recording (right) ($n = 4$). (**G** and **H**) Body weight gain (G) and cumulative energy intake (H) of female control and ERα^vlVMH-DRN-KO mice ($n = 5$ or 4). (D to H) Results are presented as means ± SEM. (D) *$P < 0.05$ in unpaired t tests. (E to H) *$P < 0.05$ and **$P < 0.01$ in two-way ANOVA analysis followed by post hoc Sidak tests.

these observations showing that DREADD activation of ERα^vlVMH neurons markedly increased BAT thermogenesis and physical activity in both male and female mice. We further expanded this discovery to show that chronic activation of ERα^vlVMH neurons protected OVX female mice from HFD-induced body weight gain, arguing that activity of these ERα^vlVMH neurons can have a meaningful impact on the body weight regulation. Combining the observation that E2 directly activates ERα^vlVMH neurons, our findings support a model that estrogen activates ERα^vlVMH neurons to stimulate both BAT thermogenesis and physical activity, therefore preventing body weight gain.

In the present study, we further identified that 5-HT^DRN neurons represent a key downstream neural node mediator of ERα^vlVMH actions on BAT thermogenesis and physical activity. We first used a WGA-GFP anterograde tracer to show that ERα^vlVMH neurons send projections to the DRN, where they exclusively innervate 5-HT neurons. Further, implementing rabies monosynaptic retrograde tracing, as well as the CAV2 retrograde tracing, we provide complementary evidence for these ERα^vlVMH → DRN projections. We used CRACM to functionally confirm that ERα^vlVMH neurons provide monosynaptic glutamatergic inputs to 5-HT^DRN neurons. At the physiological level, we used both ChR2-mediated and DREADD-mediated circuit activation to demonstrate stimulatory effects of the ERα^vlVMH → DRN projections on BAT thermogenesis and physical activity. Notably, infusion of glutamatergic antagonists into the DRN blocked the observed stimulatory effects on BAT thermogenesis and physical activity. These results not only support a key role of glutamatergic neurotransmission in mediating these effects but also exclude potential confounding actions of other collateral projections of DRN-projecting ERα^vlVMH neurons. We used a dual DREADD approach to show that simultaneous inhibition of 5-HT^DRN neurons blocked effects of activation of ERα^vlVMH neurons, further highlighting the function of the ERα^vlVMH → 5-HT^DRN circuit on the regulations of BAT thermogenesis and physical activity.

In supporting the metabolic functions of the ERα^vlVMH → 5-HT^DRN circuit, inhibition or ablation of central 5-HT has been previously shown to disrupt temperature control (*29*, *30*). Specifically, chemogenetic activation or inactivation of 5-HT^DRN neurons resulted in a significant increase or decrease, respectively, in BAT temperature without affecting food intake (*31*). In addition, the stimulation of 5-HT^DRN neurons has been reported to exert a context-dependent control of physical activity. Optogenetic activation of 5-HT^DRN neurons suppressed movement in low and moderate threat environments but induced escape behavior in high threat settings. The movement-related 5-HT^DRN neural dynamics are also inverted in low versus high threat environments (*32*), suggesting a vital role of 5-HT^DRN neurons in the regulation of physical activity. These findings indicate that stimulation of 5-HT^DRN neurons at least partially recapitulates the increases in thermogenesis and physical activity observed when the ERα^vlVMH neurons are activated.

Optogenetic and/or chemogenetic approaches are powerful toward illustrating a robust phenotypic outcome when a neural circuit is experimentally manipulated. However, these experimental manipulations may not recapitulate the exact activity of a neural circuit in any physiological condition, and therefore, the physiological relevance of optogenetic/chemogenetic results is often hard to evaluate. To circumvent this issue, we complemented the optogenetic/chemogenetic experiments with a circuit-specific gene deletion approach. In particular, we combined a retrograde flpo vector, a flpo-dependent Cre vector, and a loxP-flanked mouse allele to achieve the deletion of an endogenous gene (encoding ERα) in a selectively targeted site (vlVMH) with a specific projection (to the DRN). Female mice lacking ERα in this subset of DRN-projecting vlVMH neurons showed reduced BAT thermogenesis and physical activity and increased susceptibility to HFD-induced obesity. These results, combined with our observations from optogenetic/chemogenetic manipulations of the ERα^vlVMH → DRN projections, highlight the physiological significance of this estrogen-sensitive vlVMH→DRN circuit in the regulation of energy homeostasis.

An important question regarding the function of ERα^{vlVMH} is whether the stimulatory effects of ERα^{vlVMH} on BAT thermogenesis depend on increased physical activity. It is well established that spontaneous physical activity contributes to thermogenesis (33, 34). The observed increased BAT thermogenesis may be a possible secondary effect induced by up-regulation of physical activity. However, our data suggest dissociated regulatory mechanisms. Although DREADD activation of ERα^{vlVMH} neurons increased both BAT thermogenesis and physical activity, the time scales of these two responses are different. In both males and females, the up-regulation of physical activity lasted about 3 hours after the CNO injection, whereas the rise of BAT thermogenesis persisted for 6 hours. Consistently, optogenetic inhibition of the ERα^{vlVMH} → DRN neural circuit decreased BAT thermogenesis but not physical activity during the lights-on period, clearly indicating independent mechanisms. While increased physical activity likely contributes partially to the increased thermogenesis, at least a portion of temperature elevations are mediated through mechanisms independent of physical activity. One potential explanation is the difference in downstream nerve systems/effectors. The temperature regulation could achieve faster than physical activity because it is a straightforward autonomic response. On the other hand, the physical activity regulation may involve synergistic effects from different inputs on the somatic nervous system and voluntary locomotor activity.

It has been long known that the medial preoptic area (MPOA) of the hypothalamus is a thermoregulatory center. A portion of MPOA neurons can be activated by warm ambient temperature (35, 36), and activation of multiple MPOA neural populations has been shown to markedly reduce body temperature (35, 37–39). Here, we found that DRN-projecting ERα^{vlVMH} neurons were activated when animals were exposed to cold, and activation of these cold-sensitive neurons robustly increased BAT thermogenesis and body temperature. While these warm- and cold-sensitive neurons in distinct hypothalamic regions oppositely respond to changes in the ambient temperature, these responses appear to function in concert to provide negative feedback mechanisms to maintain thermal homeostasis. The mechanisms by which DRN-projecting ERα^{vlVMH} neurons respond to temperature changes are unclear. Notably, the vlVMH receives robust projections from MPOA neurons (37, 40). Thus, it is possible that ERα^{vlVMH} neurons respond to changes in ambient temperature through circuitry inputs from warm-sensitive MPOA neurons. In addition, recent single-cell RNA sequencing studies revealed that vlVMH neurons express multiple temperature-sensing genes, including *Grik2*, *Trpa1*, and *Trpm8* (18), raising an alternative possibility that vlVMH neurons may directly sense temperature changes. Both of these potential mechanisms warrant future investigations.

Another interesting finding from our study was that DRN-projecting ERα^{vlVMH} neurons were inhibited by food deprivation. Considering that activation of these neurons increased thermogenesis and physical activity, both of which involve consumption of energy, we suggest that the fasting-induced inhibition of DRN-projecting ERα^{vlVMH} neurons represents a protective mechanism for animals to conserve energy when food is not available. Consistent with this idea, we recently reported that DRN-projecting ERα^{vlVMH} neurons are inhibited by decreased extracellular glucose concentrations (11). Collectively, DRN-projecting ERα^{vlVMH} neurons appear to integrate ambient temperature and nutritional/metabolic states of animals to engage adaptive responses for better survival. Notably,

we show that OVX in female mice abolished responses of these ERα^{vlVMH} neurons to cold exposure or to fasting, indicating that endogenous ovarian hormones are required to coordinate the thermoregulatory responses and nutritional states. Of course, it is broadly recognized that VMH neurons also integrate other hormonal cues, including leptin (41), insulin (42), thyroid hormones (43), and glucagon-like peptide-1 (44), to regulate thermogenesis. Considering that these hormones are tightly controlled by animals' nutritional states, it is possible that these signals also regulate the responsiveness of VMH neurons to temperature alterations, which remains to be examined.

BAT thermogenesis is predominantly governed by the sympathetic nervous system (SNS) via the ADRB3 signaling pathway (45). Rabies retrograde tracing studies have shown that multiple brain regions, including the VMH and DRN, send indirect outputs to BAT (46, 47). However, the ADRB3 antagonist failed to block or blunt increased BAT thermogenesis and physical activity induced by optogenetic activation of the ERα^{vlVMH} → DRN projections, although the ADRB3 blockade itself expectedly reduced the baseline BAT thermogenesis and physical activity. Thus, these findings suggest that the effects of the ERα^{vlVMH} → DRN circuit on thermogenesis and physical activity involve other neuronal or hormonal pathways independent of the SNS/ADRB3. These alternative pathways may include the vagal afferent (48), adrenocorticotropic hormones (49), fibroblast growth factor-21 (50), glucagon-like peptide-1 (51), etc. Additional studies are needed to examine the potential contributions of these signals.

In conclusion, we identified the ERα^{vlVMH} → DRN neural circuit as an estrogen-sensitive pathway to prevent body weight gain by stimulating BAT thermogenesis and physical activity. Notably, this circuit also integrates the nutritional states of the animals with ambient temperature to coordinate appropriate responses for better survival, a mechanism that requires intact ovarian hormones. Our results reveal how ERα neurons in female brains interact with hormonal/neuronal systems and the external environment to maintain homeostatic control of energy balance and thermoregulation. These findings advance our understanding of the neuroendocrine mechanisms underlying female metabolic health and provide a necessary framework for the development of therapeutic interventions for metabolic and/or thermoregulatory dysfunctions in females, especially in those after menopause.

METHODS
Mice
Several transgenic mouse lines were maintained on a C57BL6/J background. These lines include Esr1-Cre mice (#017911, The Jackson Laboratory, Bar Harbor, ME), TPH2-iCreER (#016584, The Jackson Laboratory), Rosa26-LSL-tdTOMATO (#007914, The Jackson Laboratory), Esr1$^{lox/lox}$ (52), and ERα-ZsGreen (19). Esr1-Cre, TPH2-iCreER, and Rosa26-LSL-tdTOMATO were crossed to generate Esr1-Cre/TPH2-iCreER and Esr1-Cre/TPH2-iCreER/Rosa26-LSL-tdTOMATO for either dual DREADD or CRACM. ERα-ZsGreen and Rosa26-LSL-tdTOMATO were crossed to generate ERα-ZsGreen/Rosa26-LSL-tdTOMATO for electrophysiological recording. Mice were housed in a temperature-controlled environment at 22° to 24°C on a 12-hour light/12-hour dark cycle (6 a.m. and 6 p.m.) or 14-hour light/10-hour dark cycle (5 a.m. and 7 p.m.). Unless otherwise stated, the mice were fed ad libitum with standard mouse chow (6.5% fat; #2920, Harlan-Teklad, Madison, WI) and water.

Neurotracing and histology

To map the downstream neurons of ERα[vlVMH] neurons, 8-week-old Esr1-Cre mice received stereotaxic injections of Ad-iN/WED to the vlVMH [200 nl, −1.5 mm anterior-posterior (AP), ±0.7 mm medial-lateral (ML), and −5.9 mm dorsal-ventral (DV)]. Because Ad-iN/WED is a Cre-dependent virus, WGA-GFP was exclusively expressed in ERα[vlVMH] neurons and anterogradely traveled along the fibers, past the synapse, and filled the downstream neurons that were innervated by ERα[vlVMH] neurons terminals. Seven days after injections, mice were perfused, and brains were coronally cut at 25 μm (five series). The sections were incubated at room temperature in primary goat anti-WGA antibody (1:1000; #AS-2024, VectorLabs, Burlingame, CA, USA) overnight, followed by the secondary donkey anti-goat Alexa Fluor 488 (1:500; #A-11055, Invitrogen, Carlsbad, CA, USA) for 1.5 hours. Subsequently, sections were incubated with a rabbit anti-5-HT antibody (1:10,000; #20080, ImmunoStar, Hudson, WI, USA), followed by secondary goat anti-rabbit Alexa Fluor 594 (1:500; #A-11037, Invitrogen). Fluorescent images were obtained using a Leica DM5500 fluorescence microscope with OptiGrid structured illumination configuration.

To establish the innervation between ERα[vlVMH] neurons and the DRN neural population, 8-week-old Esr1-Cre female mice were injected with 200 nl of AAV2-EF1a-FLEX-GT into the vlVMH. Two weeks after, 400 nl of EnVA-G–deleted Rabies-mCherry was injected in the DRN (−4.65 mm AP, ±0 mm ML, and −3.5 mm DV). One week after EnVA-G–deleted Rabies-mCherry injection, mice were perfused, and brains were coronally sectioned as described above. These brain sections were subjected to mCherry immunohistochemistry. Briefly, brain sections were incubated with rabbit polyclonal DsRed antibody (1:1000; #632496, Clontech, Mountain View, CA, USA) at room temperature overnight, followed by the biotinylated donkey anti-rabbit secondary antibody (1:1000; #711-067-003, Jackson ImmunoResearch) for 2 hours. Sections were then incubated in the avidin-biotin complex (1:1000; PK-6100, Vector Laboratories) and incubated in 0.04% 3,3′-diaminobenzidine and 0.01% hydrogen peroxide. Slides were coverslipped, and both bright-field and fluorescence images were analyzed as described above.

To further establish the innervation between vlVMH neurons and the TPH2[DRN] neural population, 8-week-old TPH2-iCreER/Rosa26-LSL-tdTOMATO female mice were injected with 200 nl of AAV2-EF1a-FLEX-GTB into the DRN. The mice then received a tamoxifen injection 3 days after virus delivery (0.2 mg/g body weight, i.p.). Two weeks after, 200 nl of EnVA-G–deleted Rabies-mCherry was injected into the DRN. Two weeks after EnVA-G–deleted Rabies-mCherry injection, mice were perfused, brains were coronally sectioned, and sections were subjected to mCherry immunohistochemistry as described above.

To examine the Cre activity in the DRN of Esr1-Cre mice, female Esr1-Cre mice were injected with AAV2-DIO-hM3Dq-mCherry into the DRN. Two weeks after surgery, mice were perfused, and brains were coronally cut at 25 μm (five series). The sections were incubated at room temperature in primary sheep anti-TPH antibody (1:1000; #AB1541, Millipore, Burlington, MA, USA) overnight, followed by the secondary Donkey Anti-Sheep Alexa Fluor 488 (1:500; #713-545-003, Jackson ImmunoResearch, West Grove, PA, USA) for 1.5 hours. Fluorescent images were obtained using a Leica DM5500 fluorescence microscope with OptiGrid structured illumination configuration.

Electrophysiology

The electrophysiological responses of identified ERα neurons in the vlVMH to 17β-estradiol (E2) treatment were investigated in ERα-ZsGreen mice as previously described (26). Briefly, whole-cell patch-clamp recordings were performed on identified green fluorescent neurons in the brain slices containing vlVMH from ERα-ZsGreen mice. Six- to twelve-week-old mice were deeply anesthetized with isoflurane and transcardially perfused with an ice-cold, carbogen-saturated (95% O_2 and 5% CO_2) sucrose-based cutting solution (pH 7.3), containing 10 mM NaCl, 25 mM $NaHCO_3$, 195 mM sucrose, 5 mM glucose, 2.5 mM KCl, 1.25 mM NaH_2PO_4, 2 mM Na pyruvate, 0.5 mM $CaCl_2$, and 7 mM $MgCl_2$. The entire brain was removed and coronally cut into slices (250 μm) with a Microm HM 650V vibratome (Thermo Fisher Scientific, Waltham, MA, USA). Then, the vlVMH-containing hypothalamic slices were incubated in oxygenated artificial cerebrospinal fluid (aCSF; adjusted to pH 7.3) containing 126 mM NaCl, 2.5 mM KCl, 2.4 mM $CaCl_2$, 1.2 mM NaH_2PO_4, 1.2 mM $MgCl_2$, 11.1 mM glucose, and 21.4 mM $NaHCO_3$ for 1 hour at 34°C.

Slices were transferred to the recording chamber and perfused at 34°C in oxygenated aCSF at a flow rate of 1.8 to 2 ml/min. ZsGreen-labeled ERα[vlVMH] neurons were visualized using epifluorescence and infrared-differential interference contrast (DIC) imaging. The intracellular solution (adjusted to pH 7.3) contained the following: 128 mM K gluconate, 10 mM KCl, 10 mM Hepes, 0.1 mM EGTA, 2 mM $MgCl_2$, 0.05 mM Na–guanosine triphosphate (GTP), and 0.05 mM Mg–adenosine triphosphate (ATP). Recordings were made using a MultiClamp 700B amplifier (Molecular Devices, Sunnyvale, CA, USA), sampled using Digidata 1440A, and analyzed offline with pClamp 10.3 software (Molecular Devices). Sseries resistance was monitored during the recording, and the values were generally <10 megohm and were not compensated. The liquid junction potential was +12.5 mV and was corrected after the experiment. Data were excluded if the series resistance increased markedly during the experiment or without overshoot for the action potential. Currents were amplified, filtered at 1 kHz, and digitized at 20 kHz. The current clamp was engaged in testing neuronal firing and resting membrane potential before and after a 1s puff of aCSF containing vehicle or 100 nM E2.

To block the majority of presynaptic inputs, the aCSF solution was supplemented with 1 μM TTX (a sodium channel blocker; #1078, R&D Systems, Minneapolis, MN, USA) and a cocktail of fast synaptic inhibitors, namely, bicuculline (50 μM, a GABA receptor antagonist; Tocris Inc., Bristol, UK), D-AP5 (30 μM, an NMDA receptor antagonist; Tocris Inc.), and CNQX (30 μM, an AMPA receptor antagonist; Tocris Inc.). D-AP5 and CNQX were used to block glutamatergic inputs, while bicuculline was included to block the γ-aminobutyric acid neuron (GABAergic) inputs. The current clamp was engaged in testing neural firing and resting membrane potential before and after a 1s puff of aCSF containing a vehicle or 100 nM E2 in the presence of TTX, bicuculline, CNQX, and D-AP5.

To assess the effect of CNO on ERα and TPH2 neurons, 8- to 10-week-old Esr1-Cre/TPH2-iCreER mice were simultaneously injected with AAV2-DIO-hM3Dq-mCherry into the vlVMH (UNC Vector Core, bilaterally 200 nl; 1.60 mm posterior, 0.70 mm lateral, and 5.90 mm ventral to the bregma, based on Franklin & Paxinos Mouse Brain Atlas) and AAV2-DIO-hM4Di-mCherry into the DRN (UNC Vector Core, 4.65 mm posterior, 0 mm lateral, and 3.60 mm ventral to the bregma) 2 to 3 weeks before recording.

Three days after virus delivery, tamoxifen (0.2 mg/g body weight) was intraperitoneally injected to induce expression of TPH2-iCreER. CNO was applied to the bath solution through perfusion as previously described (53). Effects of CNO (10 μM) on membrane potential and firing frequency of mCherry-labeled ERα and TPH2 neurons were electrophysiologically recorded.

Photostimulation-induced changes in neuronal firing and membrane potential were recorded with the whole-cell current-clamp mode. Esr1-Cre mice at 8 weeks of age were injected with AAV2-DIO-ChR2-EYFP or AAV-DIO-iC++-EYFP (UNC Vector Core) into vlVMH 2 to 3 weeks before recording. To photostimulate ChR2- or iC++-positive fibers, a blue light (473 nm, 10 ms per pulse, 10 pulses per 1 s for 6 min) was focused on the vlVMH. Effects of blue light photostimulation on membrane potential and firing frequency of ChR2- or iC++-labeled ERα^{vlVMH} neurons were electrophysiologically recorded.

The electrophysiological responses of identified DRN projecting ERα^{vlVMH} neurons to different environment temperatures were investigated in ERα-ZsGreen/Rosa26-LSL-tdTOMATO mice. Briefly, 8-week-old ERα-ZsGreen/Rosa26-LSL-tdTOMATO mice received stereotaxic injections of 400 nl of CAV2-Cre into the DRN. CAV2-Cre virus retrogradely traveled from the initial injection site to the upstream brain regions projecting to DRN. The Cre recombinase induce red fluorescent tdTOMATO expression in these upstream neurons. One week later, infected mice were exposed to different environmental temperatures including room temperature (23°C), 4°C, and 40°C for 30 min, respectively. In another experiment setting, ERα-ZsGreen mice received stereotaxic injections of 400 nl of red retrobeads into the DRN. The whole-cell patch clamp recordings were performed on identified red (tdTOMATO or retrobeads), green (ERα-ZsGreen), or dual fluorescent neurons (ERα-ZsGreen and tdTOMATO or red retrobeads) in the brain slice containing vlVMH to determine the responses of neural firing frequency and membrane potential to the changes of environmental temperature.

CRACM was used to establish a functional connection between ERα^{vlVMH} neurons and 5-HT^{DRN} neurons. Specifically, 8-week-old Esr1-Cre/TPH2-iCreER/Rosa26-LSL-tdTOMATO mice were injected with 200 nl of AAV2-DIO-ChR2-EYFP and 200 nl of Ad-iN/WED (22) into the vlVMH. The mice also received tamoxifen injection 3 days after virus delivery (0.2 mg/g body weight, i.p.) to induce expression of TPH2-iCreER, which labeled all TPH2 neurons with red fluorescence (tdTOMATO). Because Ad-iN/WED is a Cre-dependent virus, WGA-GFP was exclusively expressed in ERα^{vlVMH} neurons and anterogradely traveled along the fibers, past the synapse, and filled the downstream neurons that were innervated by ERα^{vlVMH} terminals. Seven days after injections, photostimulation of ChR2-positive fibers was induced by a blue light focused on the DRN. Then, whole-cell patch current clamp recordings were performed on identified dual fluorescent neurons (WGA-GFP and tdTOMATO) in the brain slices containing DRN to determine the responses of neuronal firing frequency and membrane potential to the photostimulation of ERα^{vlVMH} neuronal fibers in the presence of 1 μM TTX.

In addition, voltage clamping was also performed to record the eEPSC. The intracellular solution for current-clamp recordings contained 125 mM CsCH$_3$SO$_3$, 10 mM CsCl, 5 mM NaCl, 2 mM MgCl$_2$, 1 mM EGTA, 10 mM Hepes, 5 mM (Mg)ATP, and 0.3 mM (Na)GTP (pH 7.3 with NaOH). To block the majority of presynaptic inputs, the aCSF solution also contained 1 μM TTX, 4-AP (1 μM,

a potassium channel blocker), and a cocktail of fast synaptic inhibitors, including bicuculline (50 μM), D-AP5 (30 μM), and CNQX (30 μM). The eEPSC in identified dual fluorescent neurons (WGA-GFP and tdTOMATO) was measured with the voltage-clamp mode with a holding potential of −60 mV in the presence of 4-AP and TTX or CNQX and D-AP5.

DREADD manipulation of ERα^{vlVMH} neuron

To examine the metabolic effects of ERα^{vlVMH} neuron acute activation, female Esr1-Cre or WT littermates were bilaterally injected with 200 nl of AAV2-DIO-hM3Dq-mCherry into the vlVMH at 8 weeks of age. Simultaneously, a telemetry probe (E-Mitter, Starr Life Sciences Corp, Oakmont, PA, USA) was implanted inside the abdominal cavity. After a 2-week of recovery phase, CNO (3 mg/kg) was intraperitoneally injected in both control (WT + hM3Dq) and mutant mice (Esr1-Cre + hM3Dq) at 9:30 a.m. and 5:00 p.m., respectively. Body core temperature and physical activity were continuously measured by the Emitter Receiver Base during the experimental phase. After a 3-day rest period, both control and mutant mice were subjected to the same procedure but received an intraperitoneal injection of saline. Thirty days after virus injection, all mice were perfused with 10% formalin, and brains were collected. Brains were sectioned and then mounted. The mCherry signals were monitored under a fluorescent microscope for validation of injection accuracy. Only those mice with mCherry signals exclusively in the vlVMH were included in analyses for feeding behavior.

In another separate trial, both male and female Esr1-Cre or WT littermates were injected with AAV2-DIO-hM3Dq-mCherry into the vlVMH, and Emitter was implanted underneath the BAT to measure BAT temperature. Saline or CNO (3 mg/kg) was intraperitoneally injected at 9:30 a.m. BAT temperature and physical activity were continuously monitored following the same procedure.

To examine the metabolic effects of ERα^{vlVMH} neurons long-term activation, female Esr1-Cre or WT littermates were ovariectomized at 8 weeks of age and simultaneously injected with AAV2-DIO-hM3Dq-mCherry into the vlVMH. Two weeks after surgery, both WT and mutant mice received intraperitoneal injection of CNO twice a day (3 mg/kg, 9 a.m. and 5 p.m.) for 2 weeks. All mice were fed normal chow for the first week and changed to HFD for the second week. Food intake and body weight were monitored every day.

DREADD stimulation of DRN-projecting ERα^{vlVMH} neurons

Esr1-Cre female mice at 8 weeks of age were bilaterally injected with 200 nl of AAV2-DIO-hM3Dq-mCherry into the vlVMH. Simultaneously, a guide cannula (C315GS-4/SPC with a terminal length of 3.5 mm; P1 Technologies, Roanoke, VA) was implanted to aim the DRN (4.65 mm posterior, 0 mm lateral, and 3.00 mm ventral to the bregma). An internal-cannula (C200IS-5/SPC customized to fit 3.5-mm C200GS-5/SPC with 0.5-mm projection, P1 Technologies) was used for drug infusion. Under the same anesthesia, an emitter was intra-abdominally implanted. Two weeks after surgeries, mice received an intro-DRN injection of 400 nl of saline, 400 nl of CNO (1 μg/μl in saline) (54, 55), 400 nl of CNO (1 μg/μl in saline) + D-AP5 (6.25 μg/μl in saline) + CNQX (2.5 μg/μl in saline) (56), or 400 nl D-AP5 (6.25 μg/μl) + CNQX (2.5 μg/μl). Physical activity and core temperature were continuously recorded before and after infusion. The order of infusion was randomized to avoid "sequence effects," and each trial was separated by 6 days to ensure "wash out" of the previous infusion.

Dual DREADD

To directly test whether 5-HT^{DRN} neurons mediate the stimulatory effects of $ER\alpha^{vlVMH}$ neurons on BAT thermogenesis and physical activity, the dual DREADD system was applied to simultaneously activate $ER\alpha^{vlVMH}$ neurons and inhibit 5-HT^{DRN} neurons. Specifically, 200 nl of AAV2-DIO-hM3Dq-mCherry was bilaterally injected into vlVMH, while 400 nl of AAV2-DIO-hM4Di-mCherry was injected into DRN of 8-week-old Esr1-Cre/TPH2-iCreER mice. An emitter was also implanted under the BAT as described above. The mice then received a tamoxifen injection 3 days after virus delivery (0.2 mg/g body weight, i.p.). Because both viruses are Cre-dependent, hM3Dq was exclusively expressed in $ER\alpha^{vlVMH}$ neurons, while hM4Di was only expressed in 5-HT^{DRN} neurons. Two weeks after surgery, the mice were injected with CNO (3 mg/kg) at 10 a.m. to simultaneously activate $ER\alpha^{vlVMH}$ neurons and inhibit 5-HT^{DRN} neurons. Both BAT temperature and physical activity were continuously recorded before and after CNO injection. Three days later, saline was injected at 10 a.m., and BAT temperature and physical activity were recorded as a baseline. To validate accurate and sufficient infection, all mice were perfused with 10% formalin. Brain sections were obtained at 25 μm (five series) and subjected to mCherry immunohistochemistry as described above. Only those mice with mCherry signals were included in the analyses.

In another control experiment, 400 nl of AAV2-DIO-hM4Di-mCherry was injected into the DRN of TPH2-iCreER mice. The effects of 5-HT^{DRN} inhibition on BAT thermogenesis and physical activity were determined as described above.

Optogenetic inhibition/activation of $ER\alpha^{vlVMH} \rightarrow$ DRN neurons

Esr1-Cre female mice at 8 weeks of age were bilaterally injected with 200 nl of AAV-DIO-iC++-EYFP into the vlVMH. Simultaneously, a light fiber (200-nm-diameter core, numerical aperture 0.22; Thor Laboratories, Newton, NJ, USA) was implanted to target the DRN (4.65 mm posterior, 0.00 mm lateral, and 3.25 mm ventral to the bregma). Under the same anesthesia, an emitter was intra-abdominally implanted, and a temperature transponder (IPTT-300, Bio Medic Data Systems, Seaford, DE, USA) was implanted under the BAT. Two weeks after surgeries, blue light stimulation (473 nm, 10 ms per pulse, 20 Hz, 3-s on, and 2-s off for 1 hour) was used to inhibit $ER\alpha^{vlVMH} \rightarrow$ DRN neurons during the lights-on period between 8 a.m. and 9 a.m. BAT thermogenesis, core temperature, and physical activity were recorded before, during, and 1 hour after stimulation. As a control experiment, yellow light with the same modulation was applied. The intensity of light power exiting the fiber tip corresponds to 5 mW for blue and yellow light.

To determine the primary mediator for the stimulatory effects of $ER\alpha^{vlVMH} \rightarrow$ DRN circuit on BAT thermogenesis and physical activity, AAV-DIO-ChR2-EYFP was bilaterally injected into the vlVMH, and a light fiber was implanted into the DRN as described above. After surgery recovery, saline or SR59230A, a ADRB3 antagonist (0.5 mg/kg in saline; #S8688, Sigma-Aldrich, St. Louis, MO, USA) were intraperitoneally injected before blue or yellow light stimulation during lights-on period between 8 a.m. and 9 a.m., respectively. BAT thermogenesis and physical activity were monitored as described above.

As a post hoc validation, mice were perfused 90 min after yellow/blue light photostimulation in the DRN (20 Hz, 10-ms pulses, and 3-mW constant stimulation for 5 min). DRN-specific activation was validated by immunohistochemistry of cFOS (1:1000; #2250, Cell Signaling) as described above.

Construction of an AAV vector for Flp-dependent expression of Cre recombinase

An AAV carrying Cre recombinase in Flp-dependent double-inverted open reading frame, pAAV-hSyn1-frEX-Cre-GFP, was constructed using pAAV-hSyn1s-DIO-SK3-2A-GFP-bGHpA as a backbone. The following components were arranged in the downstream of left inverted terminal repeat (ITR) of the backbone: human synapsin promoter; frt; F3; inverted Cre-2A-eGFP from Cre Shine (Addgene plasmid, #37404); inverted frt; inverted F3; woodchuck hepatitis virus posttranscriptional regulatory element; bovine growth hormone poly(A) sequence; and right ITR. The AAV-hSyn1-frEX-Cre-GFP vector was packaged into serotype 2/8 through the Neuro-connectivity Core in the Jan and Dan Duncan Neurological Research Institute at Texas Children's Hospital. Flp-dependent Cre expression from pAAV-hSyn1-frEX-Cre-GFP was verified in vitro by immunofluorescence imaging for DsRed in infected human embryonic kidney 293 cells transfected with AAV-hSyn1-frEX-Cre-GFP + PGK-LSL-DsRed (Addgene plasmid, #13769) or AAV-hSyn1-frEX-Cre-GFP + CAG-Flpe (Addgene plasmid, #13787) + PGK-LSL-DsRed.

Retrograde deletion

To determine whether $ER\alpha$ expressed by $ER\alpha^{vlVMH} \rightarrow$ DRN neurons is required for estrogenic regulation of body weight control, $ER\alpha$ was retrogradely deleted from $ER\alpha^{vlVMH} \rightarrow$ DRN neurons. Specifically, 8-week-old female $Esr1^{flox/flox}$ mice received a 400-nl ΔG Rabies FLPo-dsRedXpress injection into the DRN and bilateral injections of 200 nl of AAV-hSyn1-frEX-Cre-GFP into vlVMH. An emitter was also implanted under the BAT as described above. Because ΔG Rabies FLPo-dsRedXpress is a retrograde virus, Rabies-carried FLPo-dsRed was taken up by the fiber terminals in the DRN and retrograded back to the cell body in the vlVMH. Upon injection of flpo-dependent AAV-hSyn1-frEX-Cre-GFP virus, Cre recombinase was expressed exclusively in a subset of vlVMH neurons projecting to the DRN and deleted $ER\alpha$ in these neurons. Another group of control $Esr^{flox/flox}$ mice received AAV2-GFP into the DRN and bilateral injections of AAV-hSyn1-frEX-Cre-GFP into the vlVMH. One week after virus injection, all mice were fed with a normal chow diet for 1 week and changed to HFD for 2 weeks. Food intake and body weight were measured once every other day. BAT thermogenesis and physical activity were continuously monitored for the whole experimental period. The specificity of $ER\alpha$ retrograde deletion was first validated by immunohistochemistry of $ER\alpha$ and immunofluorescent staining of dsRed. Briefly, brain sections were incubated with rabbit anti-$ER\alpha$ antibody (1:10,000; catalog no. C1355, Millipore) at room temperature overnight, followed by the biotinylated donkey anti-rabbit secondary antibody (1:1000, #711-067-003, Jackson ImmunoResearch) for 2 hours. Sections were then incubated in the avidin-biotin complex (1:1000; PK-6100, Vector Laboratories) and incubated in 0.04% 3,3′-diaminobenzidine and 0.01% hydrogen peroxide. Subsequently, brain sections were incubated with anti-dsRed–Alexa Fluor 594 antibody (1:200; catalog no. sc-390909 AF594, Santa Cruz Biotechnology) overnight. Both fluorescent and bright-field images were obtained using a Leica DM5500 microscope.

To quantify $ER\alpha$ in the vlVMH, another aliquot of brain sections was used for immunohistochemistry of $ER\alpha$ as described above.

After dehydration through graded ethanol, the slides were then immersed in xylene and coverslipped. Bright-field images were analyzed as described before.

Statistics

Statistical analyses were performed using GraphPad Prism. Methods of statistical analyses were chosen on the basis of the design of each experiment and indicated in the figure legends. The data were presented as means ± SEM. $P \leq 0.05$ was considered to be statistically significant.

Study approval

Care of all animals and procedures were approved by Baylor College of Medicine Institutional and The University of Illinois at Chicago Animal Care and Use Committee.

SUPPLEMENTARY MATERIALS

Supplementary material for this article is available at https://science.org/doi/10.1126/sciadv.abk0185

View/request a protocol for this paper from *Bio-protocol*.

REFERENCES AND NOTES

1. F. Mauvais-Jarvis, D. J. Clegg, A. L. Hevener, The role of estrogens in control of energy balance and glucose homeostasis. *Endocr. Rev.* **34**, 309–338 (2013).
2. J. Santollo, M. D. Wiley, L. A. Eckel, Acute activation of ERα decreases food intake, meal size, and body weight in ovariectomized rats. *Am. J. Physiol. Regul. Integr. Comp. Physiol.* **293**, R2194–R2201 (2007).
3. S. Ogawa, J. Chan, J. A. Gustafsson, K. S. Korach, D. W. Pfaff, Estrogen increases locomotor activity in mice through estrogen receptor α: Specificity for the type of activity. *Endocrinology* **144**, 230–239 (2003).
4. P. A. Heine, J. A. Taylor, G. A. Iwamoto, D. B. Lubahn, P. S. Cooke, Increased adipose tissue in male and female estrogen receptor-alpha knockout mice. *Proc. Natl. Acad. Sci. U.S.A.* **97**, 12729–12734 (2000).
5. Y. Xu, T. P. Nedungadi, L. Zhu, N. Sobhani, B. G. Irani, K. E. Davis, X. Zhang, F. Zou, L. M. Gent, L. D. Hahner, S. A. Khan, C. F. Elias, J. K. Elmquist, D. J. Clegg, Distinct hypothalamic neurons mediate estrogenic effects on energy homeostasis and reproduction. *Cell Metab.* **14**, 453–465 (2011).
6. A. W. Smith, M. A. Bosch, E. J. Wagner, O. K. Rønnekleiv, M. J. Kelly, The membrane estrogen receptor ligand STX rapidly enhances GABAergic signaling in NPY/AgRP neurons: Role in mediating the anorexigenic effects of 17β-estradiol. *Am. J. Physiol. Endocrinol. Metab.* **305**, E632–E640 (2013).
7. G. Pelletier, S. Li, V. Luu-The, F. Labrie, Oestrogenic regulation of pro-opiomelanocortin, neuropeptide Y and corticotrophin-releasing hormone mRNAs in mouse hypothalamus. *J. Neuroendocrinol.* **19**, 426–431 (2007).
8. S. Musatov, W. Chen, D. W. Pfaff, C. V. Mobbs, X. J. Yang, D. J. Clegg, M. G. Kaplitt, S. Ogawa, Silencing of estrogen receptor alpha in the ventromedial nucleus of hypothalamus leads to metabolic syndrome. *Proc. Natl. Acad. Sci. U.S.A.* **104**, 2501–2506 (2007).
9. P. B. Martinez de Morentin, I. Gonzalez-Garcia, L. Martins, R. Lage, D. Fernandez-Mallo, N. Martinez-Sanchez, F. Ruiz-Pino, J. Liu, D. A. Morgan, L. Pinilla, R. Gallego, A. K. Saha, A. Kalsbeek, E. Fliers, P. H. Bisschop, C. Dieguez, R. Nogueiras, K. Rahmouni, M. Tena-Sempere, M. Lopez, Estradiol regulates brown adipose tissue thermogenesis via hypothalamic AMPK. *Cell Metab.* **20**, 41–53 (2014).
10. S. M. Correa, D. W. Newstrom, J. P. Warne, P. Flandin, C. C. Cheung, A. T. Lin-Moore, A. A. Pierce, A. W. Xu, J. L. Rubenstein, H. A. Ingraham, An estrogen-responsive module in the ventromedial hypothalamus selectively drives sex-specific activity in females. *Cell Rep.* **10**, 62–74 (2015).
11. Y. He, P. Xu, C. Wang, Y. Xia, M. Yu, Y. Yang, K. Yu, X. Cai, N. Qu, K. Saito, J. Wang, I. Hyseni, M. Robertson, B. Piyarathna, M. Gao, S. A. Khan, F. Liu, R. Chen, C. Coarfa, Z. Zhao, Q. Tong, Z. Sun, Y. Xu, Estrogen receptor-α expressing neurons in the ventrolateral VMH regulate glucose balance. *Nat. Commun.* **11**, 2165 (2020).
12. C. F. Yang, M. C. Chiang, D. C. Gray, M. Prabhakaran, M. Alvarado, S. A. Juntti, E. K. Unger, J. A. Wells, N. M. Shah, Sexually dimorphic neurons in the ventromedial hypothalamus govern mating in both sexes and aggression in males. *Cell* **153**, 896–909 (2013).
13. H. Lee, D. W. Kim, R. Remedios, T. E. Anthony, A. Chang, L. Madisen, H. Zeng, D. J. Anderson, Scalable control of mounting and attack by Esr1+ neurons in the ventromedial hypothalamus. *Nature* **509**, 627–632 (2014).
14. K. Hashikawa, Y. Hashikawa, R. Tremblay, J. Zhang, J. E. Feng, A. Sabol, W. T. Piper, H. Lee, B. Rudy, D. Lin, Esr1+ cells in the ventromedial hypothalamus control female aggression. *Nat. Neurosci.* **20**, 1580–1590 (2017).
15. A. L. Falkner, P. Dollar, P. Perona, D. J. Anderson, D. Lin, Decoding ventromedial hypothalamic neural activity during male mouse aggression. *J. Neurosci.* **34**, 5971–5984 (2014).
16. D. Lin, M. P. Boyle, P. Dollar, H. Lee, E. S. Lein, P. Perona, D. J. Anderson, Functional identification of an aggression locus in the mouse hypothalamus. *Nature* **470**, 221–226 (2011).
17. J. E. van Veen, L. G. Kammel, P. C. Bunda, M. Shum, M. S. Reid, M. G. Massa, D. V. Arneson, J. W. Park, Z. Zhang, A. M. Joseph, H. Hrncir, M. Liesa, A. P. Arnold, X. Yang, S. M. Correa, Hypothalamic oestrogen receptor alpha establishes a sexually dimorphic regulatory node of energy expenditure. *Nat. Metab.* **2**, 351–363 (2020).
18. D. W. Kim, Z. Yao, L. T. Graybuck, T. K. Kim, T. N. Nguyen, K. A. Smith, O. Fong, L. Yi, N. Koulena, N. Pierson, S. Shah, L. Lo, A. H. Pool, Y. Oka, L. Pachter, L. Cai, B. Tasic, H. Zeng, D. J. Anderson, Multimodal analysis of cell types in a hypothalamic node controlling social behavior. *Cell* **179**, 713–728.e17 (2019).
19. K. Saito, Y. He, X. Yan, Y. Yang, C. Wang, P. Xu, A. O. Hinton Jr., G. Shu, L. Yu, Q. Tong, Y. Xu, Visualizing estrogen receptor-α-expressing neurons using a new ERα-ZsGreen reporter mouse line. *Metabolism* **65**, 522–532 (2016).
20. J. L. Gomez, J. Bonaventura, W. Lesniak, W. B. Mathews, P. Sysa-Shah, L. A. Rodriguez, R. J. Ellis, C. T. Richie, B. K. Harvey, R. F. Dannals, M. G. Pomper, A. Bonci, M. Michaelides, Chemogenetics revealed: DREADD occupancy and activation via converted clozapine. *Science* **357**, 503–507 (2017).
21. J. M. McGlashon, M. C. Gorecki, A. E. Kozlowski, C. K. Thirnbeck, K. R. Markan, K. L. Leslie, M. E. Kotas, M. J. Potthoff, G. B. Richerson, M. P. Gillum, Central serotonergic neurons activate and recruit thermogenic brown and beige fat and regulate glucose and lipid homeostasis. *Cell Metab.* **21**, 692–705 (2015).
22. G. W. Louis, G. M. Leinninger, C. J. Rhodes, M. G. Myers Jr., Direct innervation and modulation of orexin neurons by lateral hypothalamic LepRb neurons. *J. Neurosci.* **30**, 11278–11287 (2010).
23. D. A. Steindler, R. H. Bradley, N-[acetyl-3H] wheat germ agglutinin: Anatomical and biochemical studies of a sensitive bidirectionally transported axonal tracer. *Neuroscience* **10**, 219–241 (1983).
24. N. Kinoshita, T. Mizuno, Y. Yoshihara, Adenovirus-mediated WGA gene delivery for transsynaptic labeling of mouse olfactory pathways. *Chem. Senses* **27**, 215–223 (2002).
25. I. R. Wickersham, D. C. Lyon, R. J. Barnard, T. Mori, S. Finke, K. K. Conzelmann, J. A. Young, E. M. Callaway, Monosynaptic restriction of transsynaptic tracing from single, genetically targeted neurons. *Neuron* **53**, 639–647 (2007).
26. X. Cao, P. Xu, M. G. Oyola, Y. Xia, X. Yan, K. Saito, F. Zou, C. Wang, Y. Yang, A. Hinton Jr., C. Yan, H. Ding, L. Zhu, L. Yu, B. Yang, Y. Feng, D. J. Clegg, S. Khan, R. DiMarchi, S. K. Mani, Q. Tong, Y. Xu, Estrogens stimulate serotonin neurons to inhibit binge-like eating in mice. *J. Clin. Invest.* **124**, 4351–4362 (2014).
27. L. Petreanu, D. Huber, A. Sobczyk, K. Svoboda, Channelrhodopsin-2-assisted circuit mapping of long-range callosal projections. *Nat. Neurosci.* **10**, 663–668 (2007).
28. Y. Ootsuka, K. Kulasekara, R. C. de Menezes, W. W. Blessing, SR59230A, a beta-3 adrenoceptor antagonist, inhibits ultradian brown adipose tissue thermogenesis and interrupts associated episodic brain and body heating. *Am. J. Physiol. Regul. Integr. Comp. Physiol.* **301**, R987–R994 (2011).
29. R. S. Ray, A. E. Corcoran, R. D. Brust, J. C. Kim, G. B. Richerson, E. Nattie, S. M. Dymecki, Impaired respiratory and body temperature control upon acute serotonergic neuron inhibition. *Science* **333**, 637–642 (2011).
30. N. M. Murray, G. F. Buchanan, G. B. Richerson, Insomnia caused by serotonin depletion is due to hypothermia. *Sleep* **38**, 1985–1993 (2015).
31. Y. Han, G. Xia, D. Srisai, F. Meng, Y. He, Y. Ran, Y. He, M. Farias, G. Hoang, I. Toth, M. O. Dietrich, M. H. Chen, Y. Xu, Q. Wu, Deciphering an AgRP-serotoninergic neural circuit in distinct control of energy metabolism from feeding. *Nat. Commun.* **12**, 3525 (2021).
32. C. Seo, A. Guru, M. Jin, B. Ito, B. J. Sleezer, Y. Y. Ho, E. Wang, C. Boada, N. A. Krupa, D. S. Kullakanda, C. X. Shen, M. R. Warden, Intense threat switches dorsal raphe serotonin neurons to a paradoxical operational mode. *Science* **363**, 538–542 (2019).
33. A. M. Harris, L. R. Macbride, R. C. Foster, S. K. McCrady, J. A. Levine, Does non-exercise activity thermogenesis contribute to non-shivering thermogenesis? *J. Therm. Biol.* **31**, 634–638 (2006).
34. L. Girardier, M. G. Clark, J. Seydoux, Thermogenesis associated with spontaneous activity: An important component of thermoregulatory needs in rats. *J. Physiol.* **488** (Pt. 3), 779–787 (1995).
35. C. L. Tan, E. K. Cooke, D. E. Leib, Y. C. Lin, G. E. Daly, C. A. Zimmerman, Z. A. Knight, Warm-sensitive neurons that control body temperature. *Cell* **167**, 47–59.e15 (2016).
36. S. R. Kelso, M. N. Perlmutter, J. A. Boulant, Thermosensitive single-unit activity of in vitro hypothalamic slices. *Am. J. Physiol.* **242**, R77–R84 (1982).

37. S. Rodriguez-Cuenca, E. Pujol, R. Justo, M. Frontera, J. Oliver, M. Gianotti, P. Roca, Sex-dependent thermogenesis, differences in mitochondrial morphology and function, and adrenergic response in brown adipose tissue. *J. Biol. Chem.* **277**, 42958–42963 (2002).

38. T. M. Takahashi, G. A. Sunagawa, S. Soya, M. Abe, K. Sakurai, K. Ishikawa, M. Yanagisawa, H. Hama, E. Hasegawa, A. Miyawaki, K. Sakimura, M. Takahashi, T. Sakurai, A discrete neuronal circuit induces a hibernation-like state in rodents. *Nature* **583**, 109–114 (2020).

39. S. Hrvatin, S. Sun, O. F. Wilcox, H. Yao, A. J. Lavin-Peter, M. Cicconet, E. G. Assad, M. E. Palmer, S. Aronson, A. S. Banks, E. C. Griffith, M. E. Greenberg, Neurons that regulate mouse torpor. *Nature* **583**, 115–121 (2020).

40. L. Lo, S. Yao, D. W. Kim, A. Cetin, J. Harris, H. Zeng, D. J. Anderson, B. Weissbourd, Connectional architecture of a mouse hypothalamic circuit node controlling social behavior. *Proc. Natl. Acad. Sci. U.S.A.* **116**, 7503–7512 (2019).

41. H. Dhillon, J. M. Zigman, C. Ye, C. E. Lee, R. A. McGovern, V. Tang, C. D. Kenny, L. M. Christiansen, R. D. White, E. A. Edelstein, R. Coppari, N. Balthasar, M. A. Cowley, S. Chua Jr., J. K. Elmquist, B. B. Lowell, Leptin directly activates SF1 neurons in the VMH, and this action by leptin is required for normal body-weight homeostasis. *Neuron* **49**, 191–203 (2006).

42. S. Amir, M. Lagiorgia, R. Pollock, Intra-ventromedial hypothalamic injection of insulin suppresses brown fat thermogenesis in the anaesthetized rat. *Brain Res.* **480**, 340–343 (1989).

43. M. Lopez, L. Varela, M. J. Vazquez, S. Rodriguez-Cuenca, C. R. Gonzalez, V. R. Velagapudi, D. A. Morgan, E. Schoenmakers, K. Agassandian, R. Lage, P. B. M. de Morentin, S. Tovar, R. Nogueiras, D. Carling, C. Lelliott, R. Gallego, M. Oresic, K. Chatterjee, A. K. Saha, K. Rahmouni, C. Dieguez, A. Vidal-Puig, Hypothalamic AMPK and fatty acid metabolism mediate thyroid regulation of energy balance. *Nat. Med.* **16**, 1001–1008 (2010).

44. D. Beiroa, M. Imbernon, R. Gallego, A. Senra, D. Herranz, F. Villarroya, M. Serrano, J. Ferno, J. Salvador, J. Escalada, C. Dieguez, M. Lopez, G. Fruhbeck, R. Nogueiras, GLP-1 agonism stimulates brown adipose tissue thermogenesis and browning through hypothalamic AMPK. *Diabetes* **63**, 3346–3358 (2014).

45. W. Zhang, S. Bi, Hypothalamic regulation of brown adipose tissue thermogenesis and energy homeostasis. *Front. Endocrinol.* **6**, 136 (2015).

46. D. Richard, Cognitive and autonomic determinants of energy homeostasis in obesity. *Nat. Rev. Endocrinol.* **11**, 489–501 (2015).

47. V. Ryu, A. G. Watts, B. Xue, T. J. Bartness, Bidirectional crosstalk between the sensory and sympathetic motor systems innervating brown and white adipose tissue in male Siberian hamsters. *Am. J. Physiol. Regul. Integr. Comp. Physiol.* **312**, R324–R337 (2017).

48. C. J. Madden, E. P. Santos da Conceicao, S. F. Morrison, Vagal afferent activation decreases brown adipose tissue (BAT) sympathetic nerve activity and BAT thermogenesis. *Temperature* **4**, 89–96 (2017).

49. J. C. van den Beukel, A. Grefhorst, C. Quarta, J. Steenbergen, P. G. Mastroberardino, M. Lombès, P. J. Delhanty, R. Mazza, U. Pagotto, A. J. van der Lely, A. P. N. Themmen, Direct activating effects of adrenocorticotropic hormone (ACTH) on brown adipose tissue are attenuated by corticosterone. *FASEB J.* **28**, 4857–4867 (2014).

50. E. Hondares, M. Rosell, F. J. Gonzalez, M. Giralt, R. Iglesias, F. Villarroya, Hepatic FGF21 expression is induced at birth via PPARalpha in response to milk intake and contributes to thermogenic activation of neonatal brown fat. *Cell Metab.* **11**, 206–212 (2010).

51. S. H. Lockie, K. M. Heppner, N. Chaudhary, J. R. Chabenne, D. A. Morgan, C. Veyrat-Durebex, G. Ananthakrishnan, F. Rohner-Jeanrenaud, D. J. Drucker, R. DiMarchi, K. Rahmouni, B. J. Oldfield, M. H. Tschop, D. Perez-Tilve, Direct control of brown adipose tissue thermogenesis by central nervous system glucagon-like peptide-1 receptor signaling. *Diabetes* **61**, 2753–2762 (2012).

52. Y. Feng, D. Manka, K. U. Wagner, S. A. Khan, Estrogen receptor-alpha expression in the mammary epithelium is required for ductal and alveolar morphogenesis in mice. *Proc. Natl. Acad. Sci. U.S.A.* **104**, 14718–14723 (2007).

53. C. Zhu, P. Xu, Y. He, Y. Yuan, T. Wang, X. Cai, L. Yu, L. Yang, J. Wu, L. Wang, X. Zhu, S. Wang, P. Gao, Q. Xi, Y. Zhang, Y. Xu, Q. Jiang, G. Shu, Heparin increases food intake through AgRP neurons. *Cell Rep.* **20**, 2455–2467 (2017).

54. S. X. Luo, J. Huang, Q. Li, H. Mohammad, C.-Y. Lee, K. Krishna, A. M.-Y. Kok, Y. L. Tan, J. Y. Lim, H. Li, L. Y. Yeow, J. Sun, M. He, J. Grandjean, S. Sajikumar, W. Han, Y. Fu, Regulation of feeding by somatostatin neurons in the tuberal nucleus. *Science* **361**, 76–81 (2018).

55. T. J. Stachniak, A. Ghosh, S. M. Sternson, Chemogenetic synaptic silencing of neural circuits localizes a hypothalamus-->midbrain pathway for feeding behavior. *Neuron* **82**, 797–808 (2014).

56. D. L. Walker, G. Y. Paschall, M. Davis, Glutamate receptor antagonist infusions into the basolateral and medial amygdala reveal differential contributions to olfactory vs. context fear conditioning and expression. *Learn. Mem.* **12**, 120–129 (2005).

Science Advances

An estrogen-sensitive hypothalamus-midbrain neural circuit controls thermogenesis and physical activity

Hui YeBing FengChunmei WangKenji SaitoYongjie YangLucas IbrahimiSarah SchaulNirali PatelLeslie SaenzPei LuoPenghua LaiValeria TorresMaya KotaDevin DixitXing CaiNa QuIlirjana HyseniKaifan YuYuwei JiangQingchun TongZheng SunBenjamin R. ArenkielYanlin HePingwen XuYong Xu

View the article online
https://www.science.org/doi/10.1126/sciadv.abk0185
Permissions
https://www.science.org/help/reprints-and-permissions

Use of think article is subject to the Terms of service